



HAL
open science

Dynamics and mass transfer of rising bubbles in a homogenous swarm at large gas volume fraction

Damien Colombet, Dominique Legendre, Frederic Risso, Arnaud Cockx,
Pascal Guiraud

► **To cite this version:**

Damien Colombet, Dominique Legendre, Frederic Risso, Arnaud Cockx, Pascal Guiraud. Dynamics and mass transfer of rising bubbles in a homogenous swarm at large gas volume fraction. *Journal of Fluid Mechanics*, 2015, 763, pp.254 - 285. 10.1017/jfm.2014.672 . hal-01269183

HAL Id: hal-01269183

<https://hal.science/hal-01269183>

Submitted on 14 Jan 2021

HAL is a multi-disciplinary open access archive for the deposit and dissemination of scientific research documents, whether they are published or not. The documents may come from teaching and research institutions in France or abroad, or from public or private research centers.

L'archive ouverte pluridisciplinaire **HAL**, est destinée au dépôt et à la diffusion de documents scientifiques de niveau recherche, publiés ou non, émanant des établissements d'enseignement et de recherche français ou étrangers, des laboratoires publics ou privés.

Dynamics and mass transfer of rising bubbles in an homogenous swarm at large gas volume fraction

Damien Colombet^{1,2,3†}, Dominique Legendre^{1‡},
Frédéric Risso¹, Arnaud Cockx², Pascal Guiraud²

¹Institut de Mécanique des Fluides de Toulouse, CNRS & Université de Toulouse,
Allée Camille Soula, 31400 Toulouse, France

²Laboratoire d'Ingénierie des Systèmes Biologiques et des Procédés, CNRS,
INRA & Université de Toulouse, 135 Avenue de Rangueil, 31077 Toulouse, France

³Rhodia - SOLVAY R&I, 85 Avenue des Frères Perret, BP 62, 69192 Saint Fons, France

(Received 4 November 2014)

The present work focuses on collective effect on both bubble dynamics and mass transfer in a dense homogeneous bubble swarm for gas volume fractions α up to 30%. The experimental investigation is carried out with air bubbles rising in a square column filled with water. Bubble size and shape are determined by means of a high speed camera equipped with a telecentric lens. Gas volume fraction and bubble velocity are measured by using a dual-tip optical probe. The combination of these two techniques allows us to determine the interfacial area between the gas and the liquid. The transfer of oxygen from the bubbles to the water is measured from the time evolution of the concentration of oxygen dissolved in water, which is obtained by means of the gassing-out method. Concerning the bubble dynamics, the average vertical velocity is observed to decrease with α in agreement with previous experimental and numerical investigations, while the bubble agitation turns out to be weakly dependent on α . Concerning mass transfer, the Sherwood number is found to be very close to that of a single bubble rising at same Reynolds number, provided this latter is based on the average vertical bubble velocity, which accounts for the effect of the gas volume fraction on the bubble rise velocity. This conclusion is valid for situations where the diffusion coefficient of the gas in the liquid is very low (high Péclet number) and the dissolved gas is well mixed at the scale of the bubble. It is understood by considering that the transfer occurs at the front part of the bubbles through a diffusion layer which is very thin compared to all flow length scales and where the flow remains similar to that of a single rising bubble.

Key words: Bubbly flow, Agitation, Mass transfer.

1. Introduction

Bubbly flows are usually employed in industry when the rate of mass transfer between a gas and a liquid is limited by the diffusion of the solute in the liquid. They combine the advantages of a large interfacial area by unit of volume and of an intense liquid agitation, which enhances the mixing of solute and accelerate chemical reactions. In

† Present address: LEGI, Energetic Team, Joseph Fourier University, Grenoble, France

‡ Email address for correspondence: legendre@imft.fr

many applications, the gas volume fraction α is larger than 20% and locally reaches much larger values. Bubbles can thus not be considered as isolated and collective effects have to be accounted for.

A first major collective effect is the decrease of the average bubble rise velocity $\langle V_z \rangle$ when increasing the gas volume fraction. The prediction of the increase of the bubble drag is an important issue for industrial applications. In the literature, several experimental works have investigated this phenomenon. Among them, the experiments of Wallis (1961), who investigated a homogenous bubble swarm of air bubbles in a soapy water solution, suggest that the rise velocity scales as $\langle V_z \rangle \propto (1 - \alpha)$ up to a gas volume fraction of 30%. This scaling law was established by considering the global conservation of the mass of gas, where the gas flow rate was measured directly and the gas volume fraction was deduced from the variation of the hydrostatic pressure. Using the same procedure and making an analogy with a fluidized bed, Bridge *et al.* (1964) found a rather similar scaling, $\langle V_z \rangle \propto (1 - \alpha)^{1.39}$, for the case of a countercurrent liquid flow, with air sparged into water, glycerine/water or water/isoamyl-alcohol mixtures, for $\alpha \leq 20\%$. Wijngaarden & Kapteijn (1990) determined the mean relative velocity of air bubbles in water by means of a technique based on electric conductance measurements and found that it scaled as $(1 - 1.78\alpha)$ up to a gas volume fraction of 14%. In the presence of a liquid flow Garnier *et al.* (2002) observed that $\langle V_z \rangle$ scaled as $\alpha^{1/3}$ for $\alpha \leq 40\%$ by means of a dual-tip optical probe. For different various two-phase flow configurations, Ishii & Chawla (1979) and Rusche & Issa (2000) found more complex expressions. In order to estimate relative velocity in bubbly, droplet or particulate flows, Ishii & Chawla (1979) proposed a model based on an effective viscosity of the two-phase mixture. Rusche & Issa (2000) introduced a drag correction as a combination of a power law and an exponential function with coefficients that depend on the nature of the considered dispersed flow. Direct numerical simulations of a swarm of bubble rising in a periodic domain have also been performed. For moderate Reynolds number ($Re = O(10 - 100)$), using a front tracking method and avoiding bubble coalescences, the decrease of $\langle V_z \rangle$ with α has been confirmed for both spherical (Bunner & Tryggvason 2002*a,b*) and ellipsoidal bubbles (Bunner & Tryggvason 2003). Deformed bubbles at large Reynolds number ($Re = O(100 - 1000)$) for $\alpha \leq 45\%$ have been simulated by Roghair *et al.* (2011) who used 20 Eulerian mesh points on the surface of each bubble. They observed that the decrease of the bubble velocity was affected by the bubble Eötvös number as well as by the value of the gas volume fraction. Despite the great number of experimental and numerical attempts, no general model for the rise velocity of bubbles exists yet, owing to the complexity of bubbly flows. Experimental investigations at large gas volume fractions ($\alpha > 15\%$) with accurate determination of both the bubble geometry and velocity are thus still desirable.

A second collective effect of great significance is the modification of the interfacial rate of mass transfer when the gas volume fraction is increased. Despite the significant gas volume fractions that are present in most industrial applications, many studies make use of mass transfer models developed for isolated bubbles. These models are usually based on Higbie's penetration theory (Higbie 1935), but consider various definitions for the contact time: (i) ratio of bubble diameter to bubble rise velocity, (ii) ratio of bubble surface to rate of surface formation (Nedeltchev *et al.* 2006), or (iii) based on the eddy velocity for developed turbulent flows (Lamont & Scott 1970; Kawase *et al.* 1987; Linek *et al.* 2004). With a contact time defined as the ratio of bubble diameter to bubble rise velocity (i), the Higbie's penetration theory, is also known as the Boussinesq solution (Boussinesq 1905). Numerical simulations (Takemura & Yabe 1998; Figueroa & Legendre 2010) have shown that this analytical solution appears to be very accurate to describe interfacial

mass transfer for a single clean spherical bubble rising in a still liquid, at large bubble Reynolds and Péclet numbers. Moreover, the experiments by Alves *et al.* (2006) showed that this solution was still valid for the interfacial mass transfer of a single bubble fixed in a turbulent downward liquid flow, up to a certain dissipation rate of the turbulence. The Boussinesq solution has also been used as a closure law in Eulerian-Eulerian two-fluid simulations of industrial ozonation towers (Cockx *et al.* 1999) and aeration tanks for urban wastewater treatment (Fayolle *et al.* 2007) at low to moderate volume fractions ($\alpha \leq 10\%$). Higbie's penetration theory with a contact time based on the rate of surface formation (ii) has been found to provide a good estimate of the mass transfer rate in a pressurized bubble column for either water or organic liquids (Nedeltchev *et al.* 2007). In the same time, Higbie's penetration theory with a contact time defined with eddy velocity (iii) has been preferred by Buffo *et al.* (2012) and Petitti *et al.* (2013) to simulate gas-liquid mass transfer in stirred tank reactors.

As indicated above, Boussinesq solution is *a priori* limited to large bubble Reynolds and Péclet numbers and isolated spherical bubbles. Some corrections based on results for a single bubble have been introduced to account for the effect of finite Reynolds number (Darmana *et al.* 2005; Shimada *et al.* 2007; Ayed *et al.* 2007) and that of bubble deformation (Nedeltchev *et al.* 2007) in simulations of bubble columns. Such corrections are discussed in Takemura & Yabe (1998) and Figueroa & Legendre (2010). Reviews for mass transfer can be found in Clift *et al.* (1978) and in Michaelides (2006) for bubbles, but also for drops and particles. Most of these studies have focused on mass or heat transfer from a single inclusion. Their applicability in dense dispersed flow is an important issue.

In the last decades, a few works have focused on collective effect upon mass transfer in a bubble swarm (Koynov & Khinast 2005; Kishore *et al.* 2008; Colombet *et al.* 2011; Roghair 2012). Most of them are numerical works. Two-dimensional numerical simulations of mass transfer for different arrangements of bubbles have been performed by Koynov & Khinast (2005) for small Reynolds numbers. For the case of 3 bubbles initially aligned horizontally, the authors observed a decrease of the Sherwood number. For this particular case, they noticed that, taking into account the reduced Reynolds number, the Sherwood number stays close to that of a single bubble. They also found a decrease of the Sherwood number for the case of bubbles which were initially aligned in the vertical direction. According to Koynov & Khinast (2005), this is due to the fact that bubbles are rising in the wake of each others so that both the gradient of concentration and the interfacial mass flux are reduced. One of their conclusions is that "Mass transfer in a bubble swarm depends both on the motion of the swarm as a whole and on the motion of the individual bubbles and, in general, does not follow trends observed in the single bubble cases." For both Newtonian and non-Newtonian fluids, Kishore *et al.* (2008) used a "cell model" of two concentric spheres to study numerically the collective effect of mass transfer for a clean spherical bubble. In that simplified approach, the increase of gas volume fraction is modeled by a decrease of the bounding sphere. The results seem to suggest an increase of the Sherwood number with the increase of the gas volume fraction.

The effect of increasing the gas volume fraction on the gas-liquid mass transfer coefficient has been experimentally investigated by Colombet *et al.* (2011) for air bubble in water. Thanks to a high speed camera with a fixed focal lens, a Particle Tracking Velocimetry (PTV) method was able to measure bubble volumes, shapes and velocities for gas volume fractions from 0.45 to 16.5%. In this range, the mass transfer coefficient is found very close to that of a single bubble provided the Reynolds number is based on the mean equivalent diameter and the average rising velocity of a bubble in the swarm, which suggests a weak influence of the collective effect on the mass transfer at high Péclet number. In a recent study using direct numerical simulation, Roghair (2012) found a marginal

increase of the mass transfer coefficient k_L with the increase of the gas volume fraction for 4 mm air bubbles rising in water at $Re \leq 1070$, $Sc = 1$ and $4 \leq \alpha \leq 40\%$.

The objective of the present study is to investigate collective effect on the bubble dynamics and mass transfer in very dense homogeneous bubbly flows with controlled hydrodynamic conditions. For this purpose, accurate measurements of interfacial area, bubble diameter, deformation and rising velocity are first performed for $12.1 \leq \alpha \leq 33.9\%$. Then, oxygen mass transfer experiments are conducted for $0.7 \leq \alpha \leq 29.6\%$. The paper is organized as follows. Section 2 describes the experimental methods. Section 3 presents the dynamics of the bubbles while section 4 shows the results concerning mass transfer. Section 5 is devoted to the analysis and the discussion of the results. Section 6 summarizes the main conclusions.

2. Experimental setup and instrumentation

2.1. General description

The experimental setup is described in figure 1a. It has been previously used by Riboux *et al.* (2010) and Colombet *et al.* (2011). Bubbles are injected through stainless steel capillaries [1] in a square glass column of 15×15 cm cross-section and 100 cm high. The gas line is equipped with three different rotameters [2] and one manometer [3] to deal with a large range of gas flow rates and volume fractions. A three-way valve enables to switch from nitrogen to air [4]. The use of 841 capillaries of 15 cm long and $d_c = 0.2$ mm inner diameter ensures an homogeneous injection of bubbles of almost equal sizes.

Experiments are performed at ambient temperature and pressure ($T = 20$ °C and $P = P_{atm}$). The liquid used for all experiments is tap water filtered to remove particles larger than $15 \mu m$ [5]. As a consequence, in the regime considered, gas-liquid interfaces can be considered to be clean (Ellingsen & Risso 2001). This point has been carefully validated by measuring the terminal velocity for single bubbles. The main physical properties of the system are summarized in table 1.

2.2. Measurements of gas volume fraction and bubble velocity

The gas volume fraction α and the average vertical bubble velocity $\langle V_z \rangle$ are measured by means of a dual-tip optical fiber probe (*RBI Instrumentation*) which is introduced at the center of the column [7]. A threshold just higher than the noise level is first applied on the raw signal to define the binarized signal. An example of raw and binarized signals obtained for each fiber is presented in Fig. 3. Then, the volume fraction is determined from

$$\alpha = \frac{\sum \Delta t_{yi}}{t_{acq}}, \quad (2.1)$$

where t_{acq} is the acquisition duration, Δt_{yi} the residence time of bubble i on the probe first fiber (see Fig. 3) and $\sum \Delta t_{yi}$ the total time during which the gas phase is detected. The signal acquisition is performed with a sampling frequency of 10 kHz. A good statistical convergence and an overall accuracy better than 2% is obtained for a recording time larger than 800 s.

The vertical velocity V_{zi} of bubble i is obtained by

$$V_{zi} = \frac{d_s}{\Delta t_{12i}}, \quad (2.2)$$

where Δt_{12i} is the time elapsed between the detection of the bubble interface by the first and the second fiber (as reported in Fig. 3.) and d_s is the distance between the

two fiber tips. The main difficulty of this technique is to match two successive rising fronts corresponding to the piercing of the same bubble. Spurious unrealistic low or large velocity measurements are detected in some cases, especially when two bubbles interact close to the probe. According to the sensitivity study of Riboux (2007), values smaller than $V_{min} = 0.03 \text{ m s}^{-1}$ or larger than $V_{max} = 0.7 \text{ m s}^{-1}$ have been removed.

2.3. Measurement of bubble geometrical characteristics

The most reliable technique to determine the bubble shape is probably to process images obtained by means of a high-speed camera. A classic way to image the bubbles is to use a fixed focal lens with a thin depth of field, as done by Colombet *et al.* (2011). However, the larger the gas volume fraction, the more numerous are blurred out-of-focus bubbles in the field of view. The use of a fixed focal lens is thus limited to moderate gas volume fractions ($\alpha \leq 15\%$).

The study of collective effects in a dense bubble swarm therefore requires the development and the use of another optical technique. In the present work, we use a telecentric lens, which has the particularity to have a depth of field larger than the column width (15 cm) and a constant magnification factor all along the direction of view. The main advantage is to image bubbles with sharp contours, even in a very dense bubbly flow. The main drawback is that the increase of the field of view results in a significant reduction of the spatial resolution. In addition, it has been possible to follow individual bubbles only on a short distance. For those two reasons, the measurement of the bubble velocity is less accurate and image processing has been specifically used to measure the bubble geometrical characteristics.

The imaging set-up consists of a high speed CMOS camera (*Photron APX*, Fig. 1b) equipped with a telecentric lens (*TC-4M-172 Opto Engineering*) to visualize a window of $94 \times 94 \text{ mm}$ located at the center of the column at a distance of 150 mm above the injectors tips. The spacial resolution is $5.8 \text{ pixel mm}^{-1}$. The camera is operated at 500 images per second with an exposure time varying from $1/20000$ to $1/500 \text{ s}$ depending on the lighting intensity. Lighting is supplied by an halogen spot of 1000 W.

The recorded images are processed by using *Matlab*[®]. The bubble edges are detected by applying a threshold to the raw images in gray levels. The interior of the bubbles is then filled and small aberrant objects detected in the picture are removed. A test of convexity is done to identify cases for which the detected object corresponds to two superimposed bubbles. It consists in comparing the surface area S_{obj} of the detected object to the area S_{conv} of the smallest convex polygon that can contain the object. Only the objects with $S_{obj}/S_{conv} \geq 0.95$ are retained, the others being discard. Examples of detected contours are drawn on typical raw images in figure 2 for different gas volume fractions.

The geometrical properties of the bubbles are determined by assuming that the bubbles are oblate spheroids with a minor semi-axis a and a major semi-axis b , which are measured from the two-dimensional measured contours. The bubble aspect ratio is defined as $\chi = b/a$. The bubble volume is estimated from $V_b = 4\pi b^2 a/3$ and its equivalent diameter from

$$d = (8b^2 a)^{1/3}. \quad (2.3)$$

The bubble area S_b is estimated by (Beyer 1987)

$$S_b = \pi \frac{d^2}{4} \left(2\chi^{2/3} + \frac{\chi^{-4/3}}{\sqrt{1-\chi^{-2}}} \ln \left(\frac{1 + \sqrt{1-\chi^{-2}}}{1 - \sqrt{1-\chi^{-2}}} \right) \right). \quad (2.4)$$

In addition, an indirect determination of the bubble equivalent diameter can be obtained from the dual-tip optical probe by assuming that all the bubbles have the same

size. As recalled in Colombet (2012), for a mono-dispersed population of bubbles that impact the probe with null angle of attack, d can be expressed as a function of the average chord length $\langle y \rangle$,

$$d = \frac{3}{2} \langle y \rangle \chi^{2/3} \quad , \quad (2.5)$$

where $\langle y \rangle$ is obtained from optical probe measurements as

$$\langle y \rangle = \frac{\sum_1^n (V_{zi} \Delta t_{yi})}{n} \quad , \quad (2.6)$$

and χ from image processing. (Note that the size distribution of the bubbles will be discussed in section 3.1 from the results of image processing.)

2.4. Measurement of interfacial area

For a bubble column of total volume V_{tot} , the volumetric interfacial area, $a_I = \sum S_b / V_{tot}$, is related to the gas volume fraction, $\alpha = \sum V_b / V_{tot}$, by the relation

$$a_I = \alpha \frac{\sum S_b}{\sum V_b} \quad . \quad (2.7)$$

As indicated above, for each bubble detected, a and b are obtained from the images used to determine the bubble volume V_b and surface S_b . The volume fraction α is given by the optical probe. Then, the interfacial area a_I is determined by using Eq. (2.7).

2.5. Measurement of mass transfer

The concentration $C(z, t)$ of oxygen dissolved in water at time t and elevation z is measured by means of fast response probes: Clark type micro-sensor (*Unisense Ox50*). The technique is based on the measurement of the intensity of the electric current between an anode and an oxygen reducing cathode, which is proportional to the oxygen concentration. Calibration of oxygen probes is performed for each experiment. Since the probe response is linear on the whole range of concentration considered, a calibration is performed *in situ* by using the signal measured at the beginning (anoxic water) and the end (saturated water) of each experiment. The relative uncertainty on oxygen concentration measurements is $\pm 2\%$. In the present configuration, as shown in figure 1 [6], two oxygen probes have been placed at two different elevations z , which are reported in table 2.

As shown in Colombet *et al.* (2011), due to the moderate height of the bubble column (≤ 70 cm), the oxygen saturation concentration in the water is almost not affected by the variation of hydrostatic pressure (6.4%) or by the depletion of the oxygen concentration within the bubbles during the mass transfer (6%). Moreover, the dilution of oxygen in the bubbles induced by liquid-to-gas transfer of nitrogen at the beginning of the experiments can also be neglected (1.3%). Consequently, the oxygen mass saturation concentration C^* can be considered as constant along the z axis and equals to its value at the upper surface where the pressure is equal to that of the atmosphere ($P = P_{atm}$), so that

$$C^* = x_{O_2}^{G0} \rho_{H_2O} \frac{M_{O_2}}{M_{H_2O}} \frac{(P - P^{sat})}{He} \approx 9.08 \text{ mg L}^{-1} \quad , \quad (2.8)$$

with $x_{O_2}^{G0}$ the molar fraction of oxygen in the gas phase (dry air), $\rho_{H_2O} = \rho_L$ the density of water (kg m^{-3}), M the molar masses (kg mol^{-1}), P^{sat} the vapour pressure of water in the bubbles (Pa), He the Henry constant for oxygen in water (Pa). Equation 2.8 results from the Henry's law for oxygen in water and the Raoult's law for water in air with activity and fugacity coefficients equal to unity for both equilibria, assuming that the liquid is essentially composed of water.

The classical "gassing-out" method is used to determine the time scale of the transfer of oxygen from the bubbles to the water. This method consists in first bubbling nitrogen gas in the column in order to remove the oxygen that is initially naturally present in water. Next, without changing the inlet gas flow-rate in order to not disturb the dynamics of the bubble swarm, air is suddenly injected instead of nitrogen. The concentration of dissolved oxygen C then increases until it reaches the saturation concentration C^* .

The moderate size of the column and the bubble-induced turbulence both contribute to an efficient liquid mixing so that the liquid phase can be assumed to be perfectly mixed for each horizontal slice of the bubble column. Moreover, owing to the large gas volume fractions and interfacial areas considered in this work, the vertical mass flux of dissolved oxygen generated by the axial mixing can be neglected compared to the oxygen flux coming from the bubbles. In such conditions, the variation of the concentration of dissolved oxygen along the bubble column is given by

$$\frac{\partial C(z, t)}{\partial t} = \frac{k_L a_I}{(1 - \alpha)} (C^* - C(z, t)), \quad (2.9)$$

where k_L is the liquid-side mass transfer coefficient and a_I the interfacial area. In the present configuration, the only reason for which C depends on z comes from the delay corresponding for the time taken by the bubble to reach a given elevation z . In the following the time origin is shifted by $z/\langle V_z \rangle$ so that the concentration no more depends on z and the signals provided by the two oxygen probes are synchronized.

The analysis of the measured concentrations requires to account for the response time τ_p of the probes (Letzel *et al.* 1999; Martin *et al.* 2007). For this purpose, the oxygen probe is assumed to behave as first order system,

$$\frac{\partial C_p}{\partial t} = (1/\tau_p)(C - C_p), \quad (2.10)$$

where C is the real concentration and C_p is the value provided by the probe. The response time of each probe has been measured and found close to $\tau_p = 0.8$ s. Solving eqs. (2.10) and (2.9) for a sudden increase of the mass saturation concentration saturation from 0 to C^* at $t = 0$, it yields

$$\frac{C_p}{C^*} = 1 - \frac{1}{(\tau - \tau_p)} (\tau e^{-t/\tau} - \tau_p e^{-t/\tau_p}), \quad (2.11)$$

where the time scale τ is related to the mass transfer coefficient k_L by

$$\tau = \frac{(1 - \alpha)}{k_L a_I}. \quad (2.12)$$

2.6. Homogeneity of the bubble swarm

Our purpose is to study a stable bubble column in which there is no gradient of volume fraction and no large-scale liquid motions induced by buoyancy. The use of an array of capillary tubes guarantees that the bubbles are uniformly injected at the bottom of the column. However, increasing the gas volume fraction may lead to the development of an instability and to the transition to a churn flow. The onset of the instability depends on both the liquid height H in the column and the gas volume fraction. For $H = 70$ cm, the flow is stable up to approximately $\alpha = 10\%$. For larger values of α , the liquid height has been reduced in order to keep a stable flow. The chosen values of H are reported in table 2. With this choice, the free surface at the top of the column remains still and the gas volume fraction turns out to be uniform all over the column. Figure 4 compares the superficial gas velocity $J_G = \alpha \times \langle V_z \rangle$ obtained from $\langle V_z \rangle$ and α measured by the

optical probe and the superficial gas velocity $J_G = Q_G/S$ obtained from a gas flow rate Q_G measured from the flowmeters. The good agreement obtained between these two estimations for all gas volume fractions investigated ($0.45 \leq \alpha \leq 33.9\%$) confirms the homogeneity of the gas distribution over the column.

Another departure to the flow homogeneity may come from the fact that the bubbles need a certain distance to reach their terminal velocity and that mass transfer needs a certain time to attain a steady state. Considering a clean spherical bubble starting from rest, the relaxation time scale of the bubble velocity can be estimated by $\tau_V \approx d^2/(72\nu_L) \approx 0.06$ s, which corresponds to a distance $3\tau_V V_z \approx 5.4$ cm. Concerning the mass transfer, [Figuroa & Legendre \(2010\)](#) found a transient time $\tau_C \approx 10(d^3\chi/8)^{1/3}/V_z$ for $Re = 300$, $Sc = 10$ and $\chi = 1.2$. In our case, this leads to $\tau_C \approx 0.04$ s and $\tau_C V_z \approx 1.3$ cm. It is therefore reasonable to consider that the flow and the mass transfer are fully developed at the location of the first oxygen probes, which is at least 5.8 cm above the capillaries.

3. Characterisation of the bubbles dynamics

In this section, the bubble dynamics is characterized in terms of bubble size, velocity, deformation, interfacial area and relevant dimensionless numbers. The results obtained by means of a telecentric lens are systematically presented together with those of [Colombet *et al.* \(2011\)](#), who used a fixed focal lens in the same experimental set-up for $0.45 \leq \alpha \leq 16.5\%$. In figures 5, 6, 7 and 9b, the errorbars indicate the uncertainty related to the image resolution on the measurement of bubble size and to the measurement of α . In figures 9a, 10 and 11, errorbars indicate the uncertainty related to the measurement of $\langle d \rangle$ by considering an uncertainty of ± 0.02 m s⁻¹ on the determination of the average bubble velocity $\langle V_z \rangle$.

3.1. Equivalent diameter and interfacial area

Figure 5 shows the evolution of the average bubble equivalent diameter $\langle d \rangle$ measured from image processing (Eq. 2.3) as a function of α (\circ , \bullet). The standard deviation of the equivalent diameter measured by image processing is found to range between 11% and 21% of the average value. The bubbles are therefore almost monodisperse and eq. (2.5) can also be used to estimate the bubble diameter from optical probe signals. The values determined by this method are also plotted in figure 5 (\times). Despite the strong assumptions made, including that the probe is considered to be ideal ([Kiambi *et al.* 2001](#); [Vejrazka *et al.* 2010](#)) and that all the bubbles impact the probe with a null angle of attack, the differences between the two experimental techniques is less than 14%.

The bubble diameter is observed to increase with α because of the process of bubble formation and detachment from the capillaries. At a very low gas volume fraction, the bubble formation can be considered as quasi-static and the bubble size is controlled by the equilibrium between buoyancy and capillary forces at the tip of the capillaries. The diameter is then given by the Tate law, $d_T = [6\sigma d_c/(\Delta\rho g)]^{1/3} = 2.07$ mm, as confirmed by the measurement of the detachment of a single bubble by [Riboux *et al.* \(2010\)](#). When increasing the inlet gas velocity u_c , the balance of the forces acting on a bubble involves drag and added-mass forces ([Gaddis & Vogelpohl 1986](#); [Duhar & Colin 2006](#)). For all the range of gas volume fraction considered here, the Weber number based on the capillary inner diameter, $We_c = \rho_L u_c^2 d_c / \sigma$, stays much lower than 2 so that the jet regime is never reached and the bubble generation corresponds either to the static regime of formation or the dynamic one ([Mersmann 1977](#)). Knowing the gas-flow rate through each capillary, the bubble diameter can be estimated by using the model of [Gaddis & Vogelpohl \(1986\)](#).

The predictions of this model, which are reported in figure 5, shows the same trend as the experimental results but with an underestimation of approximately 20%. This discrepancy can be due to a collective effect of the bubbles on the formation process and to bubble coalescences that may take place just above the capillary tip as observed by Manasseh *et al.* (2008).

A log-log representation (see insert in figure 5) reveals that the evolution of $\langle d \rangle$ is well described by the succession of two power-laws:

$$\frac{\langle d \rangle - d_0}{d_0} \approx 15 \alpha \quad \text{for } \alpha \leq 2.3\% \quad (3.1)$$

$$\frac{\langle d \rangle - d_0}{d_0} \approx 2.3 \alpha^{0.5} \quad \text{for } \alpha > 2.3\% \quad (3.2)$$

where $d_0 = 2.1$ mm is the value for a single bubble detaching in the static regime from one capillary ($\alpha = 0$).

Figure 6 shows the evolution of the interfacial area as a function of the gas volume fraction. It is found to regularly increase with α according to the following empirical ~~power-law~~ power-laws

$$\frac{a_I}{a_{I0}} \approx 0.402 \alpha^{0.85} \quad \text{for } \alpha \leq 2.3\% \quad (3.3)$$

$$\frac{a_I}{a_{I0}} \approx 0.336 \alpha^{0.8} \quad \text{for } \alpha > 2.3\% \quad (3.4)$$

where $a_{I0} = S_{b0}/V_{b0} = 3011 \text{ m}^{-1}$ is the surface-to-volume ratio of a single bubble detaching in the static regime.

3.2. Bubbles velocity

3.2.1. Average velocity

During the last decade, many works have investigated the velocity of bubbles rising in a swarm (Rusche & Issa 2000; Garnier *et al.* 2002; Zenit *et al.* 2001; Riboux *et al.* 2010). All these studies report a significant decrease of the average bubble vertical velocity as the gas volume fraction increases.

Figure 7 shows the average vertical bubble velocity $\langle V_z \rangle$ as a function of α . The present results obtained with a dual optical probe (\bullet) are compared to those of Riboux *et al.* (2010) ($*$) and Colombet *et al.* (2011) (\circ) that were obtained with the same technique, and to those of Colombet *et al.* (2011) (\square) that were determined by image processing with a fixed focal lens. The velocity obtained from image processing is slightly lower, probably because the detected bubbles are not far enough from the column wall. However, all the results obtained with an optical probe collapse onto a master curve of equation

$$\langle V_z \rangle = V_{z0} [0.28 + 0.72 \exp(-15\alpha)]^{0.5}, \quad (3.5)$$

where $V_{z0} = 0.32 \text{ ms}^{-1}$ is the rise velocity of an isolated bubble formed on a single capillary in the quasi-static bubbling regime, measured by Riboux *et al.* (2010). It is remarkable that a single simple correlation is able to describe the evolution of the average bubble velocity on a such large range of gas volume fraction ($0.45 \leq \alpha \leq 29.6\%$) along which $\langle V_z \rangle$ is reduced by almost a factor of two (from 0.32 ms^{-1} to 0.17 ms^{-1}).

It is important to stress that all empirical relations relating the properties of the gas phase to the gas volume fraction that have been introduced above (eq. 3.1, 3.2, 3.3, 3.4, 3.5, 4.1, 4.3, 4.5) may depend on the particular system of gas injection used here and are therefore not universal. However, they will be of great interest to analyse and discuss the results of the present work in the following of this paper.

3.2.2. Velocity fluctuations

Figure 8 shows the variances of the bubble velocity fluctuations. Let us first discuss the variance of the velocity signal provided by the dual optical probe from this work (\circ) for α up to 30% and from Riboux *et al.* (2010) ($*$) for α up to 12%. As noted by Riboux *et al.* (2010), if the dual optical probe is an accurate technique to measure the average vertical bubble velocity, it does not provide a reliable value of the variance of the bubble vertical velocity. The reason comes from the fact that the considered bubbles are oblate spheroid which move with oscillating velocity and orientation. The fluctuations that are recorded by the dual probe are thus a complex combination of the fluctuations of the vertical velocity, orientation and shape. For that reason, the measured variance is observed to depend on the exact probe geometry. The values obtained by Riboux *et al.* (2010) with a distance between the two fiber tips of 0.5 mm is indeed significantly larger than that obtained in the present work with a fiber tip separation of 1 mm. However, the variance provided by the dual optical probe can be used to characterize the evolution with the gas volume fraction of the overall energy of agitation of the bubbles in the vertical direction. It was already noticed that the bubble vertical agitation keep a constant value up to gas volume fraction around 10% by Martínez-Mercado *et al.* (2007) and Riboux *et al.* (2010), which suggested that the energy of bubble agitation remains controlled by wake instabilities. The present results seem to show that this result holds up to $\alpha = 30\%$.

In order to have a more complete description of the bubble agitation, we have also determined the velocity variance of the horizontal and the vertical bubble velocity fluctuations by particle tracking velocimetry based on images taken with a fixed focal lens. As stated before, this imaging technique already used by Colombet *et al.* (2011) is limited to moderate volume fractions. The corresponding results are also plotted in figure 8 for α up to 16%. Both the horizontal and the vertical variances are found to be almost constant, $\langle v_z'^2 \rangle \approx 0.003 \text{ m}^2 \text{ s}^{-2}$ and $\langle v_x'^2 \rangle \approx 0.0075 \text{ m}^2 \text{ s}^{-2}$, for α up to 10%. As shown by Ellingsen & Risso (2001), the horizontal component of the fluctuant velocity of an isolated bubble evolves as $v_x' = \omega A_x \cos(\omega t)$. For the present bubble size, Riboux (2007) measured an angular frequency of $\omega = 29 \text{ rad s}^{-1}$ and a path amplitude A_x varying from 3.5 to 4.9 mm, which gives a variance $\langle v_x'^2 \rangle = (A_x \omega)^2 / 2$ from 0.005 to 0.01 $\text{m}^2 \text{s}^{-2}$, in agreement with the values found here at moderate volume fraction. When α is increased beyond 10%, the vertical variance remains constant, while the horizontal one decreases down to match the vertical value around $\alpha = 12\%$. Such a decrease of the horizontal fluctuation of the dispersed phase has already been reported in solid/liquid fluidized bed by Aguilar Corona (2008) and Aguilar Corona *et al.* (2011). It may result from hindrance effects on bubble paths when increasing α .

3.3. Bubble Reynolds, Eötvös and Weber numbers

In order to fully characterize the present flow regime, it is useful to consider the values taken by the relevant dimensionless numbers in the range of volume fractions investigated. These values can be either computed from the raw values of the measured dimensional quantities or from the empirical fits proposed in the previous sections. In the following figures, plots systematically represent raw data whereas lines corresponds to values obtained from fitted data.

Figure 9a shows the Reynolds number, $Re = \langle V_z \rangle \langle d \rangle / \nu_L$. It first increases from 670 to 780 as α increases from 0 to 2.5% and then keeps a constant value as α is further increased. The constance of the Reynolds number for $\alpha \geq 2.5\%$ results from the fact that the increase in the bubble diameter (fig. 5) is compensated by the decrease of the rise velocity (fig. 7). A similar result was observed for a volume fraction up to 10% by Martínez-Mercado *et al.* (2007), who also used a bank of capillaries to inject the bubbles.

This is an interesting property of this type of experimental setup, which allows to vary the volume fraction while keeping constant the Reynolds number.

Figure 9b shows the Eötvös number: $Eo = \Delta\rho g \langle d \rangle^2 / \sigma$. As expected from the evolution of $\langle d \rangle$, it regularly increases from 0.5 to 3.2 as α varies from 0 to 30%.

Figure 10a presents the mean bubble aspect ratio, $\langle \chi \rangle$, which is found to slightly decrease from 1.7 to 1.4. In the present regime, the bubble deformation is known to be controlled by both the Weber number (Moore 1965) and the Morton number (Legendre *et al.* 2012). Here, since we are considering a single system of fluids with constant physical properties, the Morton number is constant: $Mo = g\nu_L^4 \rho_L^2 \Delta\rho / \sigma^3 = 2.5 \times 10^{-11}$. The measured Weber number, $We = \rho_L \langle V_z \rangle^2 \langle d \rangle / \sigma$, is plotted in figure 10b. It is found to decrease from about 3.25 down to 1.8. Since the Reynolds number is almost constant, the Weber number turns out to be proportional to $\langle V_z \rangle$. The decrease of the average aspect ratio, by approximately 30%, is of the same order as that of We , and both $\langle \chi \rangle$ and We keep an almost constant value for $\alpha > 15\%$. These results are in good agreement, within 14%, with the relation proposed by Legendre *et al.* (2012) for a single bubble at low Morton number:

$$\chi = \frac{1}{1 - \frac{9}{64} We} . \quad (3.6)$$

3.4. Collective effect on bubble drag coefficient

We consider now the evolution of the bubble drag coefficient C_d with the gas volume fraction in order to analyze the collective effect of the bubbles on their rise velocity. C_d is determined from the balance between drag and buoyancy forces as

$$C_d = \frac{4}{3} \frac{\Delta\rho}{\rho_L} \frac{g \langle d \rangle}{\langle V_z \rangle^2} , \quad (3.7)$$

where g is the acceleration of gravity, the average equivalent diameter $\langle d \rangle$ is measured from image processing and the average rise velocity $\langle V_z \rangle$ from the dual-tip optical probe. The experimental results are shown in figure 11 (○, ●) as a function of the gas volume fraction. C_d is observed to increase from 0.26 for $\alpha = 0.45\%$ and $\langle d \rangle \approx 2.5$ mm to 2.4 at $\alpha = 34\%$ and $\langle d \rangle \approx 5$ mm.

In order to disentangle the effect of the bubble size to that of the gas volume fraction, it is interesting to compare the present results with those obtained for single rising bubbles of the same diameter. The drag coefficient C_{d_0} of a deformed single bubble at terminal velocity is commonly estimated by (Tomiya *et al.* 1998)

$$C_{d_0} = \frac{8}{3} \frac{Eo}{c_1 + c_2 Eo} , \quad (3.8)$$

with $c_1 = 4$ and $c_2 = 1$ according to Mendelson (1967), $c_1 = 4.28$ and $c_2 = 1.02$ according to Comolet (1979), and $c_1 = 19/3$ and $c_2 = 2/3$ for $Re > 600$ with air/water systems according to Dijkhuizen *et al.* (2010).

The corresponding values are represented by empty squares and triangles in figure 11. Starting from similar values at low gas volume fractions, C_d and C_{d_0} quickly diverge as α increases. In the present experiments, the increase of C_d turns out to mainly results from hydrodynamic bubble interactions. The collective effect of bubbles is really important and leads to a drag coefficient 2.4 times larger than that of an isolated bubble at $\alpha = 34\%$.

In the literature devoted to bubbly flows, numerous relations have been proposed to describe the evolution of the drag coefficient with the gas volume fraction. Considering air bubbles injected through a porous sparger in a column of 9.5-cm diameter filled with a soapy water solution, Wallis (1961) ~~estimated the average bubble rise velocity from the~~

measurements of the gas volume fraction and the gas flow rate in the range $3 < \alpha < 30$ %. His results lead to proposed the following correlation, for $3 < \alpha < 30$ %

$$C_d = C_{d_0}(1 - \alpha)^{-2}, \quad (3.9)$$

which was later used for one-dimensional gas-liquid modelling (Wallis 1969, p. 52). We have computed C_d using relation (3.9) with C_{d_0} from Mendelson (1967). The corresponding values are represented by a plain line in figure 11. They are in fairly good agreement with the present measurements.

Applying a mixture viscosity model to their experimental results, Ishii & Chawla (1979) (see Ishii & Zuber 1979) found the following correction to account for the effect of the gas volume fraction on the bubble drag coefficient:

$$C_d = \frac{C_{d_0}}{(1 - \alpha)} \left(\frac{1 + 17.67 [f(\alpha)]^{6/7}}{18.67 f(\alpha)} \right)^2 \quad \text{with} \quad f(\alpha) = (1 - \alpha)^{1.5}. \quad (3.10)$$

This relation is also reported in figure 11 (dashed-dotted line) by using the expression proposed by Mendelson (1967) for C_{d_0} . It predicts an evolution of C_d that is close to that of Wallis (1961) so that it is difficult to conclude which one is in the best agreement with the present results.

Garnier *et al.* (2002) experimentally investigated an homogeneous air/water bubbly flow in the presence of a co-current liquid flow for volume fractions up to 30% and Reynolds numbers from 300 to 500. They results led to

$$C_d = C_{d_0} \left(1 - \alpha^{1/3} \right)^{-2}. \quad (3.11)$$

Using again the expression proposed by Mendelson (1967) for C_{d_0} , this relation (dotted line in fig.11) is found to considerably over predict the effect of the gas volume fraction upon the drag coefficient compared to the present results.

Roghair *et al.* (2011) performed numerical simulations of a bubble swarm in a periodic cubic domain for $1 \leq \text{Eo} \leq 5$, $4 \times 10^{-12} \leq \text{Mo} \leq 2 \times 10^{-9}$ and $\alpha \leq 45\%$. From their results, they proposed the following relation

$$C_d = C_{d_0} \left(1 + \frac{18}{\text{Eo}} \alpha \right), \quad (3.12)$$

where C_{d_0} is given by the relation proposed by Dijkhuizen *et al.* (2010). This relation suggests that the collective effect of the bubbles on the drag coefficient may depend on other parameters than the gas volume fraction, such as the Eötvös number. The corresponding values of C_d are represented by a dashed line in figure 11. They are about 30% higher than the present experimental data, just at the limit of the measurement uncertainty.

4. Mass transfer

In this section, the measured mass transfer coefficients and Sherwood numbers are first presented as a function of the gas volume fraction. Then, they are compared to available correlations for a single bubble rising in a liquid at rest. Finally, they are compared to transfer rates expected in a highly turbulent flow. In figures 13, 14 and 15, errorbars indicate the uncertainty related to the measurement of the interfacial area a_I , the gas volume fraction α , the bubble equivalent diameter $\langle d \rangle$ by considering an uncertainty of $\pm 10\% \tau$ on the determination of the mass transfer time scale τ .

4.1. Experimental results

The time evolutions of the oxygen concentration are presented in figure 12 for $\alpha = 1.46\%$ (a), $\alpha = 15.1\%$ (b) and $\alpha = 26.9\%$ (c). In this figure, the time origin has not been shifted by $z/\langle V_z \rangle$ so that the signal of the upper probe is delayed compared to the first one. The least squares method is used to fit each set of experimental data by eq. (2.11) in order to obtain the transfer time scale τ . The corresponding fitting curves, represented by lines in figure 12, describe accurately the experimental results, confirming that the assumptions made about the probe response and the fact that the flow is well mixed are fulfilled.

A total of 76 experimental runs have been conducted in the range of $0.7 \leq \alpha \leq 29.6\%$. The corresponding values of τ are reported in figure 13 together with the 29 values measured by of Colombet *et al.* (2011) in the range from $0.45 \leq \alpha \leq 16.5\%$. The time necessary to reach the saturation is significantly affected by the void fraction since it decreases of more than one order of magnitude between $\alpha = 1\%$ and $\alpha = 30\%$. Such a strong decrease is expected from the strong increase of the interfacial area with α (fig. 6). As it is clearly visible in the log-log plot proposed in the insert of figure 12, the experimental values of τ nicely follow a simple power law,

$$\tau \approx \tau_0 \alpha^{-0.8} \quad \text{with} \quad \tau_0 = 2.22 \text{ s} . \quad (4.1)$$

In order to analyze the collective effect of the bubbles on the mass transfer, we have to consider the mass transfer coefficient by unit of area, k_L . The experimental value of k_L is obtained from the measured values of τ , α and a_I by

$$k_L = \frac{(1 - \alpha)}{\tau a_I} . \quad (4.2)$$

Combining relations (3.4) for a_I and (4.1) for τ , the following simple empirical relation is found for the mass transfer coefficient, for $\alpha > 2.3\%$

$$k_L \approx k_{L_0} (1 - \alpha) \quad \text{with} \quad k_{L_0} = 4.45 \times 10^{-4} \text{ ms}^{-1} . \quad (4.3)$$

Figure 14a shows the evolution of the experimental values of k_L as a function of the gas volume fraction. The decrease is considerably lower compared to that of τ , which indicates that most of the evolution of the total rate of transfer results from the trivial effect of the augmentation of the interfacial area and justifies the efforts made to obtain an accurate determination of a_I .

To go further in the analysis of the physical mechanism underlying the mass transfer, we have to make dimensionless the rate of mass transfer by introducing the Sherwood number

$$Sh = \frac{k_L \langle d \rangle}{D_L} , \quad (4.4)$$

where D_L is the diffusion coefficient of dissolved oxygen in water. Figure 14b shows the evolution of the experimental Sherwood number as a function of α , which using empirical fits Eq. 3.1-3.2, 4.3 and 4.4 can be described by the following empirical relation, for $\alpha > 2.3\%$

$$Sh \approx Sh_0 (1 - \alpha) (1 + 2.3 \alpha^{0.5}) \quad \text{with} \quad Sh_0 = 445 . \quad (4.5)$$

The increase of $\langle d \rangle$ almost compensates the decrease of k_L so that Sh turns out to increase moderately with the gas volume fraction, its values remaining between 600 and 750 in the whole range of α investigated.

The present results therefore suggest that the collective effect of the bubbles has a relatively weak influence on the interfacial mass transfer considering the huge effect observed on the transfer time scale τ . However, it is difficult to conclude from the sole evolution of the Sherwood number since variations of bubble size, velocity and shape are associated to variation of gas volume fractions. In next section, we will compare the present results to those corresponding to a single bubble in the same flow regime and with the same geometrical properties.

4.2. Comparison with a single bubble rising in a liquid at rest

In most studies of mass transfer in bubble columns, the rate of transfer is estimated by using the Higbie's penetration theory (Higbie 1935),

$$k_L = \frac{2}{\sqrt{\pi}} \sqrt{\frac{D_L}{t_c}}, \quad (4.6)$$

where t_c is taken equal to $\langle d \rangle / \langle V_z \rangle$. In fact this is equivalent to the analytical solution obtained by (Boussinesq 1905) by considering that the flow around the bubble can be approximated by the potential flow and a very thin concentration layer on the bubble

$$\text{Sh} = \frac{2}{\sqrt{\pi}} Pe^{1/2}, \quad (4.7)$$

where $Pe = \langle d \rangle \langle V_z \rangle / D_L$ is the Péclet number. This solution is thus valid in the limit of large Re and Pe .

Various improvements have been proposed to account for the effect of bubble deformation or finite Reynolds number upon the mass transfer from a single bubble. Considering the flow approximation of Moore (1963), Winnikow (1967) derived the following expression that includes the effect of the Reynolds number:

$$\text{Sh} = \frac{2}{\sqrt{\pi}} \left[1 - \frac{2.89}{\sqrt{Re}} \right]^{1/2} Pe^{1/2}. \quad (4.8)$$

Measuring the mass transfer of almost spherical millimeter-sized bubbles from volume variations, Takemura & Yabe (1998) proposed the following relation,

$$\text{Sh} = \frac{2}{\sqrt{\pi}} \left[1 - \frac{2}{3} \frac{1}{(1 + 0.09 Re^{2/3})^{3/4}} \right]^{1/2} (2.5 + Pe^{1/2}) \quad (4.9)$$

which was found to be in good agreement with both experiments and numerical simulations at moderate Re numbers and large Pe .

Recently, considering numerical results from various previous works, Colombet *et al.* (2013) proposed the following relation that is valid for a spherical bubble whatever the value of Re and Pe ,

$$\text{Sh} = 1 + \left[1 + \left(\frac{4}{3\pi} \right)^{2/3} (2 Pe_{max})^{2/3} \right]^{3/4}, \quad (4.10)$$

where Pe_{max} is the Péclet number based on the maximal velocity U_{max} of the liquid at the interface instead of the bubble velocity V_z , which is obtained from the correlation proposed by Legendre (2007),

$$\frac{U_{max}}{V_z} = \frac{1}{2} \frac{16 + 3.315 Re^{1/2} + 3 Re}{16 + 3.315 Re^{1/2} + Re}. \quad (4.11)$$

When Pe tends to zero, relation (4.10) tends to the diffusive solution in the absence of

flow ($Sh = 2$) while it tends towards the Boussinesq solution when Re and Pe become very large.

The effect of the bubble deformation has been studied by [Lochiel & Calderbank \(1964\)](#), who considered the potential flow around a spheroidal bubble. They proposed to correct the Boussinesq expression by the introduction of a function f of the aspect ratio χ ,

$$Sh(\chi) = \frac{2}{\sqrt{\pi}} Pe^{1/2} f(\chi) . \quad (4.12)$$

The validity of this solution has been recently discussed by [Figueroa & Legendre \(2010\)](#), who proposed the following expression

$$f(\chi) = 0.524 + 0.88\chi - 0.49\chi^2 + 0.086\chi^3 , \quad (4.13)$$

which is based on the results of direct numerical simulations, and proved to be valid for $500 < (\chi/8)^{1/3} Re < 1000$, $\nu_L/D_L > 100$ and $1 \leq \chi \leq 3$.

The values of k_L predicted by all these expressions derived for an isolated bubble are reported in figure 14a while the corresponding values of Sh are reported in figure 14b. Because the Reynolds number remains almost constant and the bubble shape does not evolves so much in the present experiments, the predictions of all these correlations are close to each others. Moreover, these predictions are all in agreement with the experiments, considering the measurement uncertainty.

We can therefore conclude that the mass transfer in an homogeneous bubble swarm at high Péclet number is almost independent of the gas volume fraction. It has been proved to remain similar to that of a single bubble rising in a fluid at rest up to a volume fraction of 30%. This conclusion is in agreement with the trends of the numerical simulations of [Roghair \(2012\)](#).

4.3. Comparison with the interfacial transfer in highly turbulent flows

The bubbles generate strong velocity fluctuations in the liquid phase. It is thus interesting to compare the rate of transfer measured here to that induced at a plane interface by a turbulence of similar intensity. It has been shown that turbulent eddies can enhance the mass transfer by causing the renewal of the liquid close to the interface ([Magnaudet & Calmet 2006](#)). Considering that the timescale t_c of renewal of the liquid at the interface is proportional to $(\nu_L/\langle\epsilon_L\rangle)^{1/2}$, where ϵ_L is the rate of dissipation of the turbulence, equation (4.6) gives

$$Sh = c_1 \left(\frac{d \langle\epsilon_L\rangle^{1/4}}{\nu_L^{3/4}} \right) Sc^{1/2} , \quad (4.14)$$

where $Sc = \nu_L/D_L$ is the Schmidt number. Several values have been proposed for the prefactor c_1 : 0.4 ([Lamont & Scott 1970](#)), 0.523 ([Linek et al. 2004](#)) or $2/\sqrt{\pi}$ ([Kawase et al. 1987](#)).

In an homogeneous bubbly flow, [Riboux et al. \(2010\)](#) showed that the rate of dissipation of the energy is given by

$$\langle\epsilon_L\rangle \approx \frac{\Delta\rho}{\rho_L} \alpha \langle V_z \rangle g . \quad (4.15)$$

According to (4.15), $\langle\epsilon_L\rangle$ ranges from 0.02 to 0.5 m^2s^{-3} for the range of gas volume fraction considered here. The Sherwood numbers given by relation (4.14) are plotted in figure 15. They are clearly not in agreement with the present measurements. Combining

eqs. (4.15) and (4.14), it yields

$$\text{Sh} = c_1 (\text{Eo}^3/\text{Mo})^{1/8} \alpha^{1/4} \text{Re}^{1/4} \text{Sc}^{1/2} . \quad (4.16)$$

The evolution of Sherwood number with the gas volume fraction predicted by this relation ($\alpha^{1/4}$) is not compatible with the experimental result. Moreover, the predicted evolution with the Reynolds number ($\text{Re}^{1/4}$) is contradictory to the scaling of expected considering the evolution for an isolated bubble ($\text{Re}^{1/2}$).

This analysis confirms that the mass transfer in the bubble column is controlled by the mass transfer around a single bubble in fluid at rest. The fact that the liquid agitation may play a negligible role in the mass transfer at a bubble interface has already been noticed by [Alves *et al.* \(2006\)](#), who investigated the case of a single bubble in a turbulent flow with a dissipation rate of one order of magnitude smaller than in the present configuration.

5. Discussion

Hydrodynamic interactions between bubbles have a strong effect on the average bubble rise velocity, which is found to decrease strongly when increasing the gas volume fraction. The analysis of the interactions between two rising bubbles in a liquid at rest reveals opposite effects depending on the relative position of the bubbles. For two bubbles rising in line, the drag force on the trailing bubble is diminished ([Yuan & Prosperetti 1994](#); [Harper 1997](#); [Ruzicka 2000](#); [Hallez & Legendre 2011](#)), so that vertical interactions between bubbles should increase the average bubbles velocity in a bubble swarm. On the other hand, the drag coefficient of two bubbles rising side by side is increased ([Legendre *et al.* 2003](#); [Hallez & Legendre 2011](#)), so that transversal interactions between bubbles should decrease the average bubble velocity. In a two-dimensional high-Reynolds-number swarm of bubbles confined between two vertical plates ([Bouche *et al.* 2012](#)), vertical interactions are predominant and both the average and the variance of the vertical bubble velocity is observed to increase with the gas volume fraction. The main difference between this configuration and the present one is that turbulence cannot develop because of the wall friction. In a three-dimensional unconfined bubble swarm, hydrodynamic interactions between bubble wakes cause a strong attenuation of individual wakes ([Risso *et al.* 2008](#)). The combination of the wake attenuation with the existence of an intense agitation of both the bubbles and the liquid phase reduces considerably the vertical entrainment by bubbles and explains why the hindering effect is predominant when the gas volume fraction increases. More surprising is the weak influence of hydrodynamic interactions on the variance of the vertical bubble agitation, which is observed to remain close to that of an isolated bubble. Even if bubble path oscillations become erratic, the fluctuant energy of their motion seems still controlled by wake instabilities.

The major finding of the present work is the absence of any significant collective effect of the bubbles on the mass transfer up to volume fraction of 30%. This result is not valid for any dispersed two-phase flow. Collective effect on the mass transfer are known to exist for a long time ([Ranz & Marshall 1952](#)). In the 60's and the 70's, many experimental works on mass (or heat) transfer in fixed or fluidized bed measured an increase of the Sherwood (or Nusselt) number with the particle volume fraction α_S ([Ranz & Marshall 1952](#); [Rowe & Claxton 1965](#); [Littman & Silva 1970](#); [Turner & Otten 1973](#); [Gunn & Souza 1974](#); [Miyachi *et al.* 1976](#); [Gunn 1978](#)). More recently, numerical simulations have confirmed this trend: [Massol \(2004\)](#) for $0 \leq \text{Re} \leq 300$, $0.72 \leq \nu/D \leq 2$, and $\alpha_S \leq 60\%$, and [Deen *et al.* \(2012\)](#) for $36 \leq \text{Re} \leq 144$, $\nu/D = 0.8$ and $\alpha_S = 30\%$,

who found results in agreement with [Gunn \(1978\)](#). The point is therefore to understand the absence of collective effect in homogenous bubbly flows.

First, let us discuss the mechanism of mass transfer for a single rising bubble. For large Reynolds and Péclet numbers, [Figuroa & Legendre \(2010\)](#) showed that the mass transfer mainly takes place across a thin diffusive layer located at the front part of the bubble, where the flow is potential. The thickness δ_D of the concentration boundary layer can be estimated from ([Boussinesq 1905](#))

$$\frac{\delta_D}{d} \approx \frac{\sqrt{\pi}}{2} Pe^{-1/2}. \quad (5.1)$$

In the present experiments, the Péclet number is around 3.5×10^5 and δ_D is of the order of $10^{-3} d$ ($\approx 5 \mu\text{m}$). In order that the solution for a single bubble can apply, two conditions must be fulfilled. First, the average flow in the close surrounding of each bubble have to be similar to that of a isolated bubble. Second, liquid velocity fluctuations must not penetrate within the concentration boundary layer. Experimental investigations of the flow around a bubble immersed within an homogeneous bubble swarm ([Risso & Ellingsen 2002](#); [Roig & Larue de Tounemine 2007](#); [Risso *et al.* 2008](#)) have shown that the first condition is satisfied; in particular, at high bubble Reynolds number, the flow in front of the bubble is well described by the potential solution for a single bubble. The second condition requires that both the distance δ_x between the interfaces of neighbour bubbles and the size of the smallest turbulent eddies η_K are large compare to the thickness δ_D of the concentration boundary layer.

If bubbles were arranged on a periodic face-centred cubic network, the minimum distance between two bubble interfaces is given by

$$\frac{\delta_x}{d} = \left(\frac{1}{\sqrt{2}} \left(\frac{2\pi}{3\alpha} \right)^{1/3} - 1 \right), \quad (5.2)$$

which gives $\delta_x \approx 0.35 d \approx 1.6 \text{ mm}$ for $\alpha = 30\%$.

As suggested by [Riboux *et al.* \(2010\)](#), the Kolmogorov microscale of the bubble-induced turbulence, which corresponds to the size of the smallest turbulent eddies, can be roughly estimated by

$$\eta_K = \left(\frac{\nu_L^3}{\langle \epsilon_L \rangle} \right)^{1/4}, \quad (5.3)$$

where the average dissipation rate $\langle \epsilon_L \rangle$ is determined from [\(4.15\)](#) and gives $\eta_K \approx 10^{-2} d \approx 50 \mu\text{m}$ for $\alpha = 30\%$. Both δ_x and η_K are therefore much larger than δ_D and the second condition is satisfied.

With a Péclet number of 1070, the results of [Roghair \(2012\)](#) did not show any collective effect. However, in the cases considered by [Massol \(2004\)](#) ($Pe = 600$) and [Deen *et al.* \(2012\)](#) ($Pe = 115$), the mass transfer was observed to depend on the volume fraction of the dispersed phase. This confirms that a large enough Péclet number is necessary so that the mass transfer is not influenced by hydrodynamic interactions.

6. Concluding remarks

Thanks to an original method of imaging using a telecentric lens and a dual optical probe, the properties of the gas phase have been measured in an homogenous swarm of bubble up to a volume fraction of 30%. In particular, the bubble deformation is found in good agreement with the correlation proposed by [Legendre *et al.* \(2012\)](#) for a single bub-

ble. Also, the average bubble velocity is observed to strongly decreases with α and found in agreement with the correlations of Wallis (1961) and Ishii & Chawla (1979). Even if some open questions remain concerning the physical mechanism responsible for the increase of the drag coefficient, available correlations are reliable to predict the deformation and the average bubble rise velocity in an homogenous bubble swarm at large Reynolds number. The bubble fluctuating velocity has also been characterized. Surprisingly, no significant influence of the gas volume fraction on the variance measured by means of the dual optical probe was observed. Hydrodynamic interactions between bubbles make the bubble path oscillations to become irregular, but they do not seem to modify the overall amount of fluctuating energy, which remains controlled by the instability of the wake behind each bubble.

The total mass transfer of oxygen from the bubbles to the liquid has been measured by means of the gassing-out method. Thanks to the determination of the total interfacial area by imaging, the mass transfer rate by unit of area and the Sherwood number have been obtained. Remarkably, the Sherwood number is found very close to that of a single bubble rising at same velocity. The reason lies in the fact that the mass flux occurs in a very thin layer located in front of the bubble. Owing to the large value of the Péclet number ($> 10^5$), the distance between the interfaces of the bubbles and the smallest turbulent eddies are much larger than the thickness of the concentration boundary layer. Consequently, the flow within this layer is not affected by the presence of the other bubbles. Moreover, the mixing generated by the bubble-induced agitation of the liquid ensures that the dissolved oxygen is homogeneous everywhere out of this layer. For the mass transfer the conditions are therefore equivalent to those of a single bubble rising in a fluid at rest and at uniform concentration. Correlations for the Sherwood number established for single rising bubbles are therefore relevant to predict the mass transfer in an homogenous bubble column up to a volume fraction of 30%, provided the bubble Reynolds and Péclet numbers are large enough. This conclusion is consistent with the results obtained experimentally for a similar system by Colombet *et al.* (2011) for gas volume fractions lower than 17% and with the numerical simulations of Roghair (2012) for a Péclet number around one thousand. Results obtained at lower Péclet number in fluidized beds however showed an increase of the Sherwood number compared to that of a single particle. There is probably a lower limit below which mass transfer in a dispersed two-phase flow depends on the volume fraction. The determination of this limit, which probably depends on parameters such as the nature of the dispersed phase or the Reynolds number, requires further investigations.

The authors would like to thank Rhodia, member of the SOLVAY Group, for supporting this work and especially Dr. C. Daniel and Dr. S. Galinat. We also thank Sébastien Cazin for its invaluable help on image processing and Grégory Ehses for his help in adapting the experimental set-up for this study. This research was carried out within the framework of a CIFREANRT contract in collaboration with the FERMaT federation.

REFERENCES

- AGUILAR CORONA, A. 2008 Agitation des particules dans un lit fluidisé liquide : Etude expérimentale. PhD thesis, Toulouse University, France.
- AGUILAR CORONA, A., ZENIT, R. & MASBERNAT, O. 2011 Collisions in a liquid fluidized bed. *Int. J. Multiphase Flow* **37** (7), 695–705.
- ALVES, S., VASCONCELOS, J. & ORVALHO, S. P. 2006 Mass transfer to clean bubbles at low turbulent energy dissipation. *Chem. Eng. Sci.* **61**, 1334 – 1337.
- AYED, H., CHAHED, J. & ROIG, V. 2007 Hydrodynamics and mass transfer in a turbulent buoyant bubbly shear layer. *AIChE J.* **53**, 2742–2753.
- BEYER, W. H. 1987 *Standard Mathematical Tables*, 28th edn. Boca Raton, CRC Press.
- BOUCHE, E., ROIG, V., RISSO, F. & BILLET, A. M. 2012 Homogeneous swarm of high-reynolds-number bubbles rising within a thin gap. part 1: Bubble dynamics. *J. Fluid Mech.* **794**, 211–231.
- BOUSSINESQ, J. 1905 Calcul du pouvoir refroidissant des courants fluides. *J. Math. Pures Appl.* **6**, 285–332.
- BRIDGE, A., LAPIDUS, L. & ELGIN, J. 1964 The mechanics of vertical gas-liquid fluidized system i : countercurrent flow. *AIChE J.* **10** (6), 819–826.
- BUFFO, A., VANNI, M. & MARCHISIO, D. L. 2012 Multidimensional population balance model for the simulation of turbulent gas-liquid systems in stirred tank reactors. *Chem. Eng. Sci.* **70**, 31–44.
- BUNNER, B. & TRYGGVASON, G. 2002a Dynamics of homogeneous bubbly flows, part 1. rise velocity and microstructure of the bubbles. *J. Fluid Mech.* **466**, 17–52.
- BUNNER, B. & TRYGGVASON, G. 2002b Dynamics of homogeneous bubbly flows, part 2. velocity fluctuations. *J. Fluid Mech.* **466**, 53–84.
- BUNNER, B. & TRYGGVASON, G. 2003 Effect of bubble deformation on the properties of bubbly flows. *J. Fluid Mech.* **495**, 77–118.
- CLIFT, R., GRACE, J. R. & WEBER, M. E. 1978 *Bubbles, drops and particules*. San Diego, Academic Press.
- COCKX, A., DO-QUANG, Z., LINÉ, A. & ROUSTAN, M. 1999 Use of computational fluid dynamics for simulating hydrodynamics and mass transfer in industrial ozonation towers. *Chem. Eng. Sci.* **54**, 5085–5090.
- COLOMBET, D. 2012 Modélisation de réacteurs gaz-liquide de type colonne à bulles en conditions industrielles. PhD thesis, Toulouse University.
- COLOMBET, D., LEGENDRE, D., COCKX, A. & GUIRAUD, P. 2013 Mass or heat transfer inside a spherical gas bubble at low to moderate reynolds number. *Int. J. Heat Mass Transfer* **67**, 1096–1105.
- COLOMBET, D., LEGENDRE, D., COCKX, A., GUIRAUD, P., RISSO, F., DANIEL, C. & GALINAT, S. 2011 Experimental study of mass transfer in a dense bubble swarm. *Chem. Eng. Sci.* **66**, 3432–3440.
- COMOLET, R. 1979 Sur le mouvement d’une bulle de gaz dans un liquide. *Houille Blanche* **1**, 31–42.
- DARMANA, D., DEEN, N. G. & KUIPERS, J. A. M. 2005 Detailed modeling of hydrodynamics, mass transfer and chemical reactions in a bubble column using a discrete bubble model. *Chem. Eng. Sci.* **60**, 3383 – 3404.
- DEEN, N. G., KRIEBITZSCH, S. H. L., VAN DER HOEF, M. A. & KUIPERS, J. A. M. 2012 Direct numerical simulation of flow and heat transfer in dense fluid-particle systems. *Chem. Eng. Sci.* **81**, 329–344.
- DIJKHUIZEN, W., ROGHAIR, I., VAN SINT ANNALAND, M. & KUIPERS, J. A. M. 2010 Dns of gas bubbles behaviour using an improved 3d front tracking model-drag force on isolated bubbles and comparison with experiments. *Chem. Eng. Sci.* **65** (4), 1415–1426.
- DUHAR, G. & COLIN, C. 2006 Dynamics of bubble growth and detachment in a viscous shear flow. *Phys. Fluids* **18** (077101).
- ELLINGSEN, K. & RISSO, F. 2001 On the rise of an ellipsoidal bubble in water: oscillatory paths and liquid-induced velocity. *J. Fluid Mech.* **440**, 235–268.
- FAYOLLE, Y., COCKX, A., GILLOT, S., ROUSTAN, M. & HEDUIT, A. 2007 Oxygen transfer prediction in aeration tanks using cfd. *Chem. Eng. Sci.* **62**, 7163–7171.

- FIGUEROA, B. & LEGENDRE, D. 2010 Mass or heat transfer from spheroidal gas bubbles rising through a stationary liquid. *Chem. Eng. Sci.* **65**, 6296 – 6309.
- GADDIS, E. S. & VOGELPOHL, A. 1986 Bubble formation in quiescent liquids under constant flow conditions. *Chem. Eng. Sci.* **41**, 97–105.
- GARNIER, C., LANCE, M. & MARIÉ, J. L. 2002 Measurement of local flow characteristics in buoyancy-driven bubbly flow at high void fraction. *Exp. Therm. Fluid Sci.* **26**, 811–815.
- GUNN, D. J. 1978 Transfer of heat or mass to particles in fixed and fluidized beds. *Int. J. Heat Mass Transfer* **21**, 467.
- GUNN, D. J. & SOUZA, J. F. C. 1974 Heat transfer and axial dispersion in packed beds. *Chem. Eng. Sci.* **29**, 1363.
- HALLEZ, Y. & LEGENDRE, D. 2011 Interaction between two spherical bubbles rising in a viscous liquid. *J. Fluid Mech.* **673**, 406–431.
- HARPER, J. F. 1997 Bubbles rising in line: why is the first approximation so bad? *J. Fluid Mech.* **351**, 289–300.
- HIGBIE, R. 1935 The rate of absorption of a pure gas into a still liquid during short periods of exposure. *Trans. Am. Inst. Chem. Eng.* **31**, 365 – 389.
- ISHII, M. & CHAWLA, T. C. 1979 Local drag laws in dispersed two-phase flow. *Technical Report, Argonne National Lab., IL (USA)*.
- ISHII, M. & ZUBER, N. 1979 Drag coefficient and relative velocity in bubbly, droplet or particulate flow. *AIChE J.* **25-5**, 843–855.
- KAWASE, Y., HALARD, B. & MOO-YOUNG, M. 1987 Theoretical prediction of volumetric mass transfer coefficients in bubble columns for newtonian and non-newtonian fluids. *Chem. Eng. Sci.* **42**, 1609–1617.
- KIAMI, S. L., DUQUENNE, A. M., BASCOUL, A. & DELMAS, H. 2001 Measurements of local interfacial area : application of bi-optical fibre technique. *Chem. Eng. Sci.* **56**, 6447–6453.
- KISHORE, N., CHHABRA, R. P. & ESWARAN, V. 2008 Bubble swarms in power-law liquids at moderate reynolds numbers: Drag and mass transfer. *Chem. Eng. Res. Des.* **86** (1), 39–53.
- KOYNOV, A. & KHINAST, J. G. 2005 Mass transfer and chemical reactions in bubble swarms with dynamic interfaces. *AIChE J.* **51** (10), 2786–2800.
- LAMONT, J. C. & SCOTT, D. S. 1970 An eddy cell model of mass transfer into the surface of a turbulent liquid. *AIChE J.* **16**, 513–519.
- LEGENDRE, D. 2007 On the relation between the drag and the vorticity produced on a clean bubble. *Phys. Fluids* **19**, 018102.
- LEGENDRE, D., MAGNAUDET, J. & MOUGIN, G. 2003 Hydrodynamic interactions between two spherical bubbles rising side by side in a viscous liquid. *J. Fluid Mech.* **497**, 133–166.
- LEGENDRE, D., ZENIT, R. & VELEZ-CORDERO, J. R. 2012 On the deformation of gas bubbles in liquids. *Phys. Fluids* **24**, 043303.
- LETZEL, H. M., SCHOUTEN, J. C., KRISHNA, R. & VAN DEN BLEEK C. M. 1999 Gas holdup and mass transfer in bubble column reactors operated at elevated pressure. *Chem. Eng. Sci.* **54**, 2237–2246.
- LINEK, V., KORDAC, M., FUJASOVA, M. & MOUCHA, T. 2004 Gas liquid mass transfer coefficient in stirred tanks interpreted through models of idealized eddy structure of turbulence in the bubble vicinity. *Chem. Eng. Process.* **43**, 1511–1517.
- LITTMAN, H. & SILVA, D. E. 1970 Gas-particle heat-transfer coefficients in packed beds at low reynolds numbers. Fourth International Heat Transfer Conference, Paris-Versailles, France.
- LOCHIEL, A. C. & CALDERBANK, P. H. 1964 Mass transfer in the continuous phase around axisymmetric bodies of revolution. *Chem. Eng. Sci.* **19**, 471–484.
- MAGNAUDET, J. & CALMET, I. 2006 Turbulent mass transfer through a flat shear-free surface. *J. Fluid Mech.* **553**, 115–185.
- MANASSEH, R., RIBOUX, G. & RISSO, F. 2008 Sound generation on bubble coalescence following detachment. *Int. J. Multiphase Flow* **34**, 938 – 949.
- MARTIN, M., MONTES, F. J. & GALAN, M. A. 2007 Bubble coalescence at sieve plates: Ii. effect of coalescence on mass transfer. superficial area versus bubble oscillations. *Chem. Eng. Sci.* **62**, 1741–1752.
- MARTÍNEZ-MERCADO, J., PALACIOS-MORALES, C. A. & ZENIT, R. 2007 Measurement of pseudoturbulence intensity in monodispersed bubbly liquids for $10 \leq \text{Re} \leq 500$. *Phys. Fluids* **19**, 103302.1–103302.13.

- MASSOL, A. 2004 Simulations numériques d'écoulements au travers des réseaux fixes de sphères monodisperses et bidisperses, pour des nombres de reynolds modérés. PhD thesis, INP Toulouse, France.
- MENDELSON, H. D. 1967 The prediction of bubble terminal velocities from wave theory. *AIChE J.* **13**, 250–253.
- MERSMANN, A. 1977 Auselegung und massstrabsvergrosserung von blasen und tropfensaulen. *Chemie Ingenieur Technik* **49**, 679–691.
- MICHAELIDES, E. E. 2006 *Particles, bubbles and drops: their motion, heat and mass transfer*.
- MIYAUCHI, T., KATAOKA, H. & KIKUCHI, T. 1976 Gas film coefficient of mass transfer in low peclet number region for sphere packed beds. *Chem. Eng. Sci.* **31**, 9.
- MOORE, D. W. 1963 The boundary layer on a spherical gas bubble. *J. Fluid Mech.* **16**, 161–176.
- MOORE, D. W. 1965 The velocity rise of distorted gas bubbles in a liquid of small viscosity. *J. Fluid Mech.* **23**, 749–766.
- NEDELTCHEV, S., JORDAN, U. & SCHUMPE, A. 2006 Correction of the penetration theory applied to the prediction of kla in a bubble column with organic liquids. *Chem. Eng. Technol.* **29**, 1113–1117.
- NEDELTCHEV, S., JORDAN, U. & SCHUMPE, A. 2007 Correction of the penetration theory based on mass-transfer data from bubble columns operated in the homogeneous regime under high pressure. *Chem. Eng. Sci.* **62**, 6263 – 6273.
- PETITTI, M., VANNI, M., MARCHISIO, D. L., BUFFO, A. & PODENZANI, F. 2013 Simulation of coalescence, break-up and mass transfer in a gas-liquid stirred tank with cqmom. *Chem. Eng. J.* **228**, 1182–1194.
- RANZ, W. E. & MARSHALL, W. R. 1952 Evaporation from drops. *Chem. Eng. Prog.* **48** (4), 173.
- RIBOUX, G. 2007 Hydrodynamique d'un essaim de bulles en ascension. PhD thesis, INP Toulouse, France.
- RIBOUX, G., RISSO, F. & LEGENDRE, D. 2010 Experimental characterization of the agitation generated by bubbles rising at high reynolds number. *J. Fluid Mech.* **643**, 509–539.
- RISSO, F. & ELLINGSEN, K. 2002 Velocity fluctuations in a homogeneous dilute dispersion of high-reynolds-number rising bubbles. *J. Fluid Mech.* **453**, 395–410.
- RISSO, F., ROIG, V., AMOURA, Z., RIBOUX, G. & BILLET, A. M. 2008 Wake attenuation in large reynolds number dispersed two-phase flows. *Phil. Trans. R. Soc. A* **366**, 2177–2190.
- ROGHAIR, I. 2012 Direct numerical simulations of hydrodynamics and mass transfer in dense bubbly flows. PhD thesis, Eindhoven University of Technology.
- ROGHAIR, I., LAU, Y. M., DEEN, N. G., SLAGTER, H. M., BALTUSSEN, M. W., VAN SINT ANNALAND, M. & KUIPERS, J. A. M. 2011 On the drag force of bubbles in bubble swarms at intermediate and high reynolds numbers. *Chem. Eng. Sci.* **66** (14), 3204–3211.
- ROIG, V. & LARUE DE TOUNEMINE, A. 2007 Measurement of interstitial velocity of homogeneous bubbly flows at low to moderate void fraction. *J. Fluid Mech.* **572**, 87–110.
- ROWE, P. N. & CLAXTON, K. T. 1965 Heat and mass transfer from a single sphere to fluid flowing through an array. *T. I. Chem. Eng.-Lond.* **43**, 321–331.
- RUSCHE, H. & ISSA, R. I. 2000 The effect of voidage on the drag force on particules, droplets and bubbles in dispersed two-phase flow. *Tech. Rep.*. BRITE-EURAM III program.
- RUZICKA, M. C. 2000 On bubbles rising in line. *Int. J. Multiphase Flow* **26**, 1141–1181.
- SHIMADA, N., TOMIYAMA, A. & OZAKI, T. 2007 Numerical prediction of bubbly flow in a bubble column with chemisorption. *ICMF, Leipzig, Germany*.
- TAKEMURA, F. & YABE, A. 1998 Gas dissolution process of spherical rising bubbles. *Chem. Eng. Sci.* **53**, 2691–2699.
- TOMIYAMA, A., KATAOKA, I., ZUN, I. & SAKAGUCHI, T. 1998 Drag coefficients of single bubbles under normal and micro gravity conditions. *JSME Int J., Ser. B* **41** (2), 472–479.
- TURNER, G. A. & OTTEN, L. 1973 Values of thermal (and other) parameters in packed beds. *Ind. Eng. Chem. Proc. D. D.* **12** (4), 417–424.
- VEJRAZKA, J., SECHET, P., VECER, M., ORVALHO, S., RUZICKA, M. & CARTELLIER, A. 2010 Measurement accuracy of a mono-fiber optical probe in a bubbly flow. *Int. J. Multiphase Flow* **36** (7), 533–548.
- WALLIS, G. B. 1961 Some hydrodynamic aspects of two-phase flow and boiling. *Int. Heat Transfer Conference, Boulder, Colorado USA* **2**, 319–325.

- WALLIS, G. B. 1969 *One dimensional two-phase flow*. McGraw Hill.
- WIJNGAARDEN, L. VAN & KAPTEIJN, C. 1990 Concentration waves in dilute bubble/liquid mixtures. *J. Fluid Mech.* **212**, 111–137.
- WINNIKOW, S. 1967 Letters to the editor. *Chem. Eng. Sci.* **22**, 22–477.
- YUAN, H. & PROSPERETTI, A. 1994 On the in-line motion of two spherical bubbles in a viscous fluid. *J. Fluid Mech.* **278**, 325–349.
- ZENIT, R., KOCH, D. L. & SANGANI, A. S. 2001 Measurements of the average properties of a suspension of bubbles rising in a vertical channel. *J. Fluid Mech.* **429**, 307–342.

ρ_L	998.2	$kg\ m^{-3}$
μ_L	$1.0038\ 10^{-3}$	$Pa\ s$
ρ_G	1.2	$kg\ m^{-3}$
μ_G	$18\ 10^{-6}$	$Pa\ s$
σ	$73\ 10^{-3}$	$N\ m^{-1}$
D_L	$2.1\ 10^{-9}$	$m^2\ s^{-1}$
He	$4.05\ 10^9$	Pa
P^{sat}	2337	Pa
M_{H_2O}	$18.015\ 10^{-3}$	$kg\ mol^{-1}$
M_{O_2}	$32\ 10^{-3}$	$kg\ mol^{-1}$
$x_{O_2}^{G0}$	20.9%	–

TABLE 1. System properties at $T = 20\ ^\circ C$ and $P = 101\ 325\ Pa$.

α (%)	H (cm)	lower probe (cm)	upper probe (cm)
$\alpha < 11$	76	14.0	69.5
$11 \leq \alpha < 21$	64.2	14.0	55.0
$21 \leq \alpha < 31$	35.2	5.8	34.8
$31 \leq \alpha < 32$	29.5	–	–
$\alpha \geq 32$	19.4	–	–

TABLE 2. Liquid height H at $\alpha = 0$ and elevation of the oxygen probes above capillaries tips.

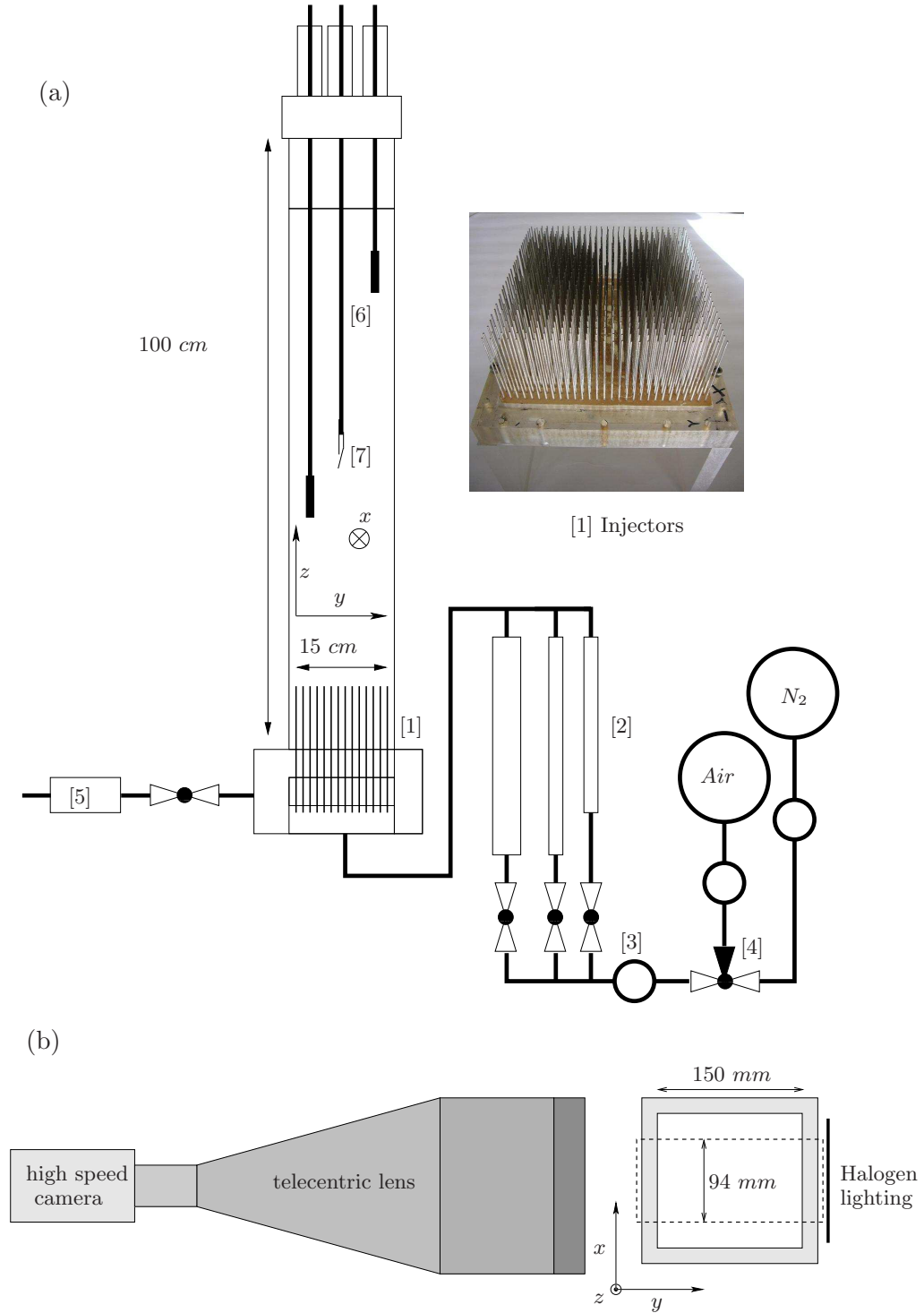


FIGURE 1. (a) Experimental installation and (b) imaging set-up.

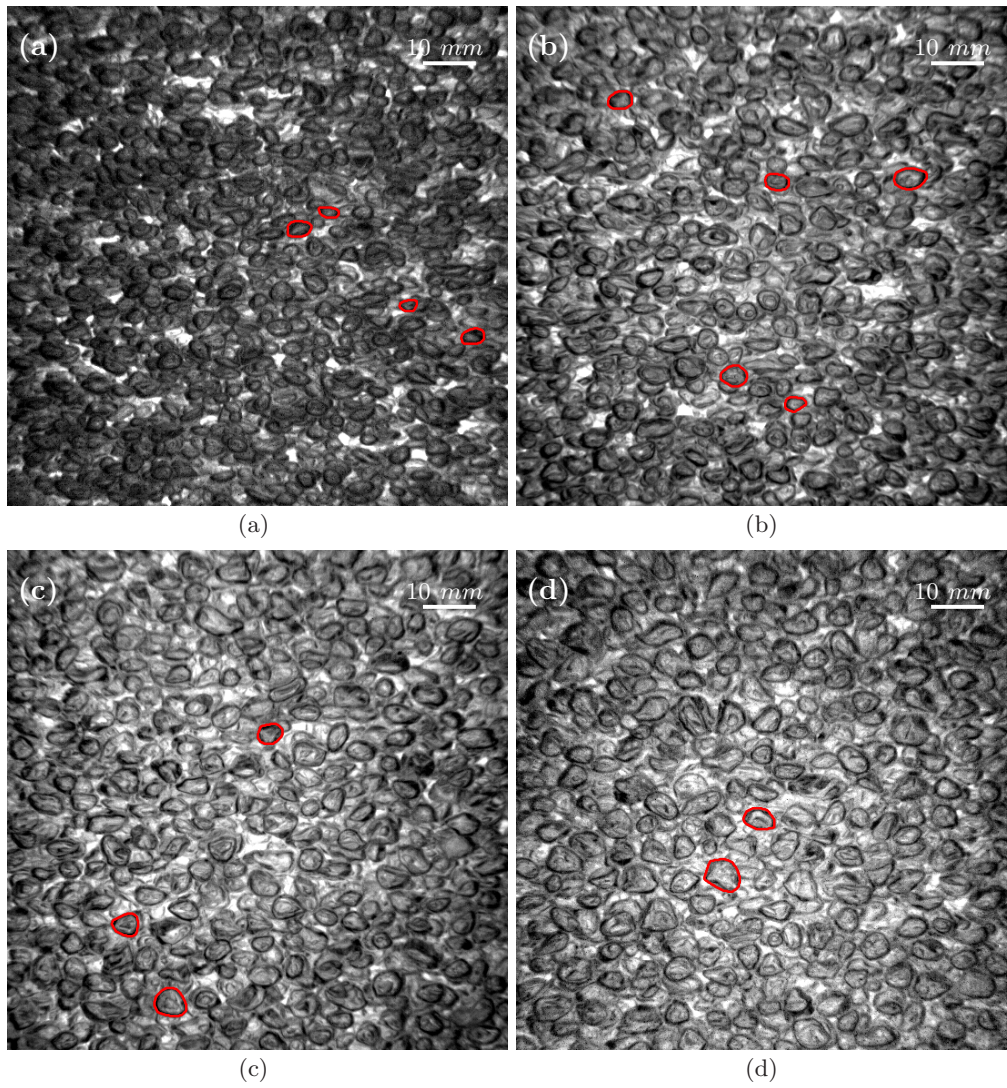


FIGURE 2. (Colour online) Typical images of the bubble swarm with detected bubble contour marked by a red line: (a) $\alpha = 12.2\%$, (b) $\alpha = 23.9\%$, (c) $\alpha = 30.6\%$, (d) $\alpha = 33.9\%$.

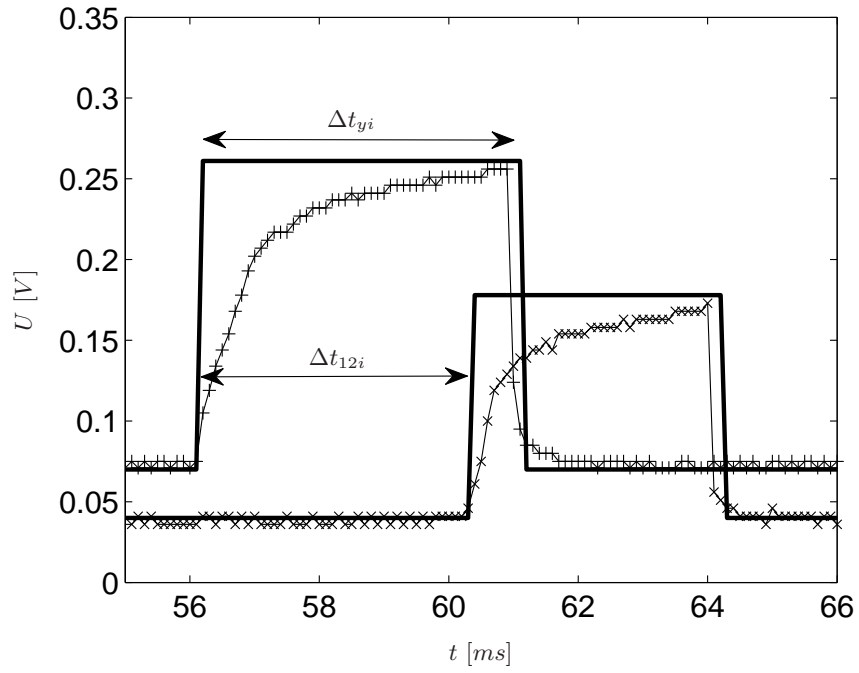


FIGURE 3. Signals from the optical probes. Symbols: raw signal from first (+) and second (x) probe. Line: binarized signals (—).

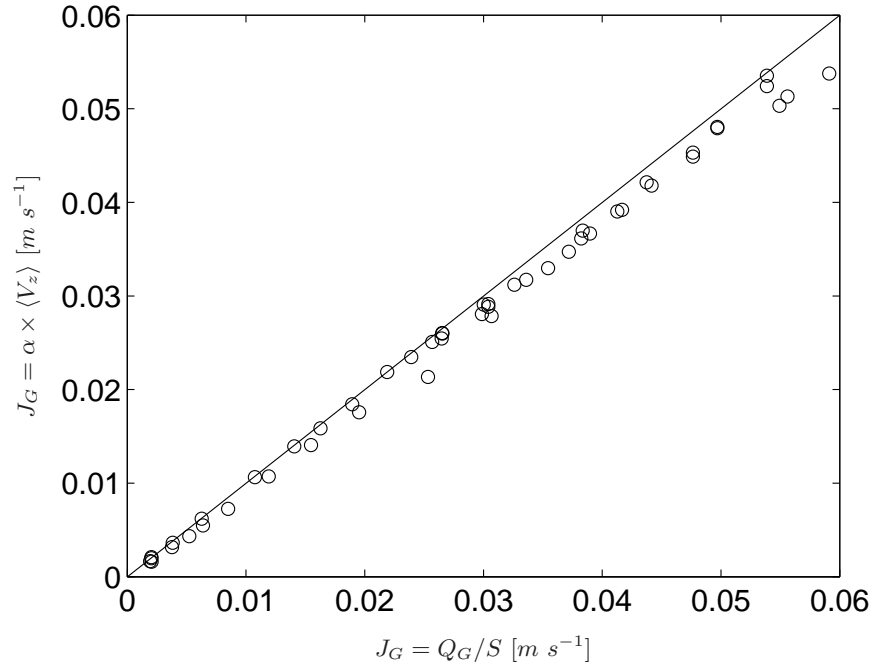


FIGURE 4. Superficial gas velocity from gas volume fraction and bubble average rising velocity measured by the dual-tip optical probe $J_G = \alpha \times \langle V_z \rangle$ versus superficial gas velocity from measured gas flow rate $J_G = Q_G/S$.

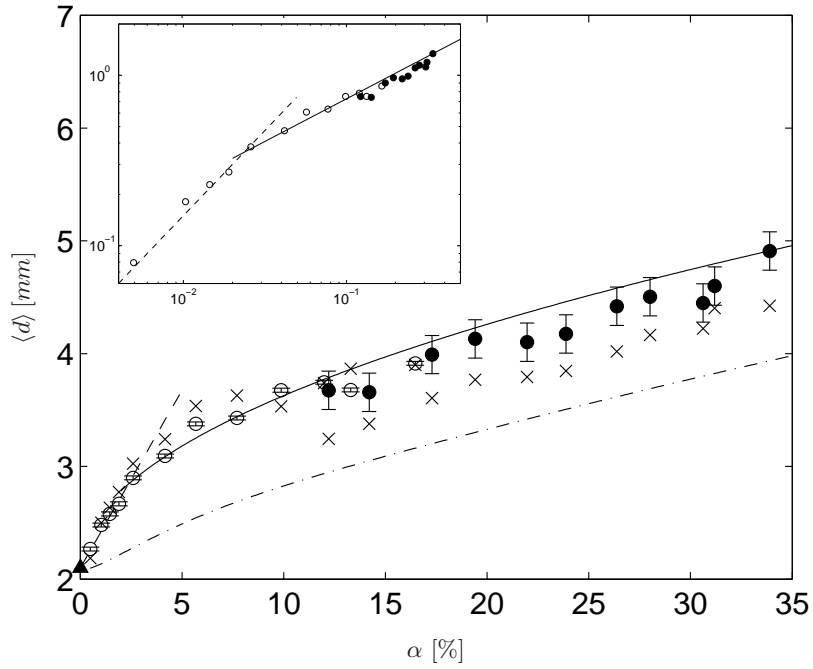


FIGURE 5. Average bubble equivalent diameter as a function of the gas volume fraction. • image processing with a telecentric lens; ○ image processing with a fixed focal lens by Colombet *et al.* (2011); × dual-tip optical probe measurements from average bubble chords (Eq. 2.5); - - equation 3.1; — equation 3.2; -.- dynamic bubble formation model of Gaddis & Vogelpohl (1986). Insert: log-log representation of $(\langle d \rangle - d_0)/d_0$ versus α .

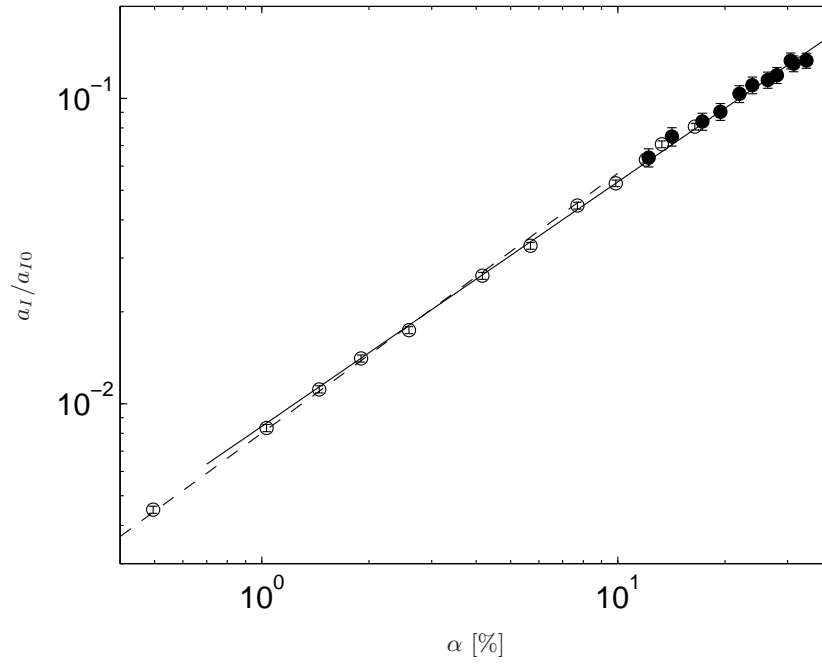


FIGURE 6. Interfacial area (Eq. 2.7) versus gas volume fraction: \bullet this work; \circ from Colombet *et al.* (2011); $--$ equation 3.3; $-$ equation 3.4.

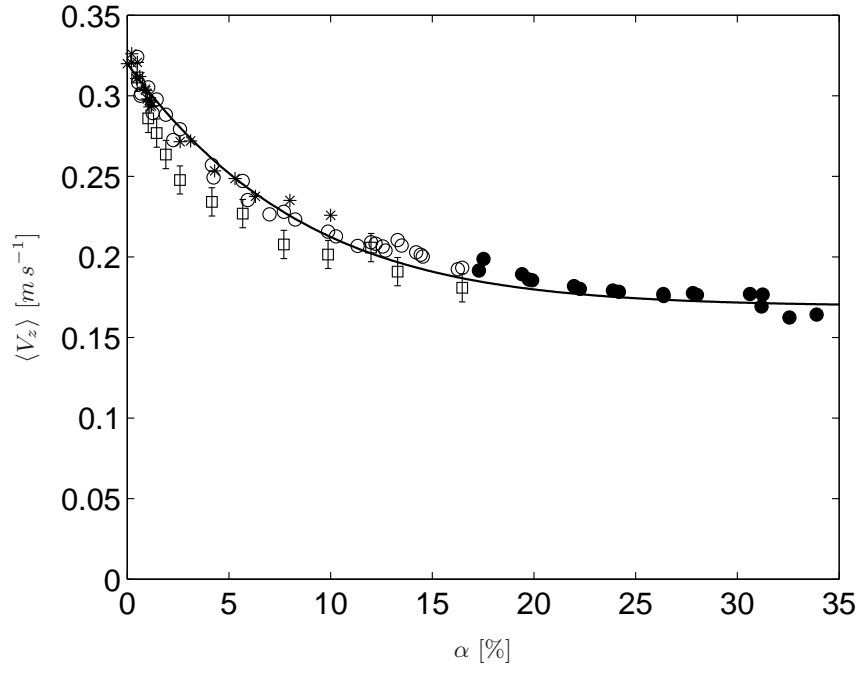


FIGURE 7. Average bubble velocity against the gas volume fraction. Dual-tip optical probe measurements from this work (\bullet), Colombet *et al.* (2011) (\circ), Riboux *et al.* (2010) (*). Particle Tracking Velocimetry by image processing from Colombet *et al.* (2011) (\square). — equation (3.5).

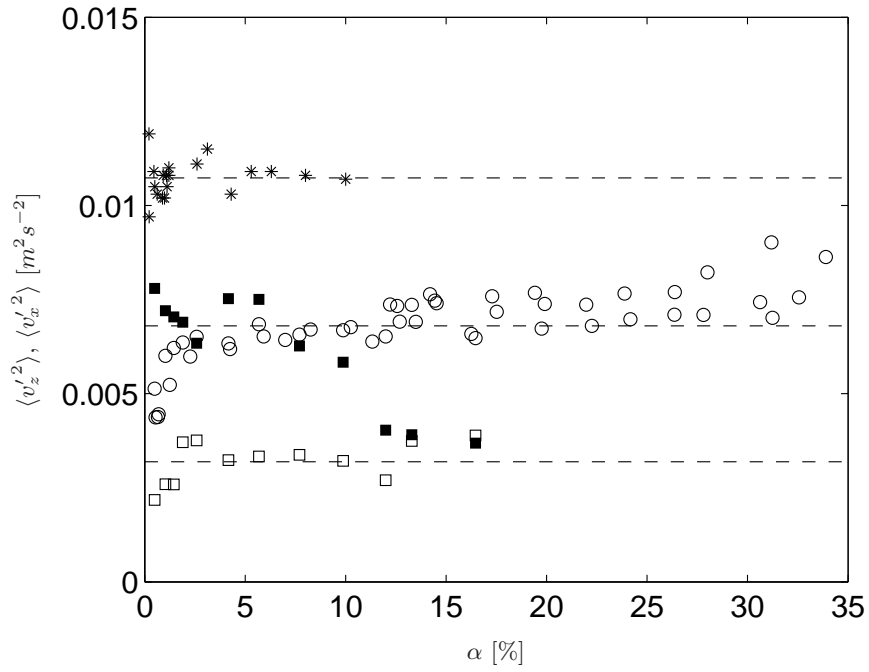


FIGURE 8. Variances of bubble velocity against gas volume fraction. Variance obtained from the dual optical probe in this work (o) and by Riboux *et al.* (2010) (*). Variances of the vertical velocity (□) and the horizontal velocity (■) measured in this work from particle tracking on images taken with a **fixed** focal lens.

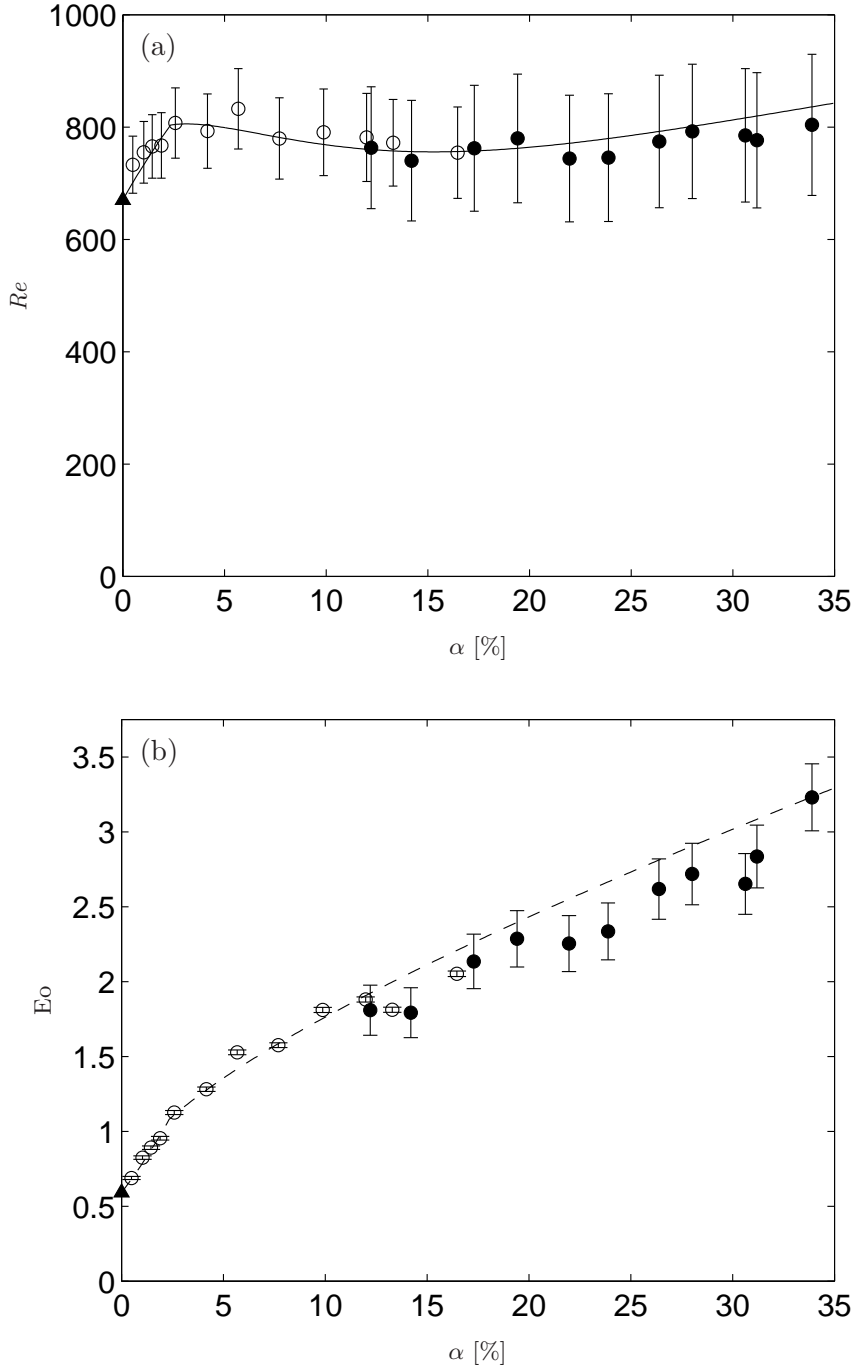


FIGURE 9. (a) Bubble Reynolds number ($Re = \langle V_z \rangle \langle d \rangle / \nu_L$) and (b) Eötvös number ($Eo = \Delta \rho g \langle d \rangle^2 / \sigma$) versus gas volume fraction: \circ method using a fixed focal lens; \bullet method using a telecentric lens; \blacktriangle result for a single bubble from Riboux *et al.* (2010); — Reynolds number determined from fitted data (eqs. 3.1, 3.2 and 3.5); -- Eötvös number determined from fitted data (eqs. 3.1 and 3.2).

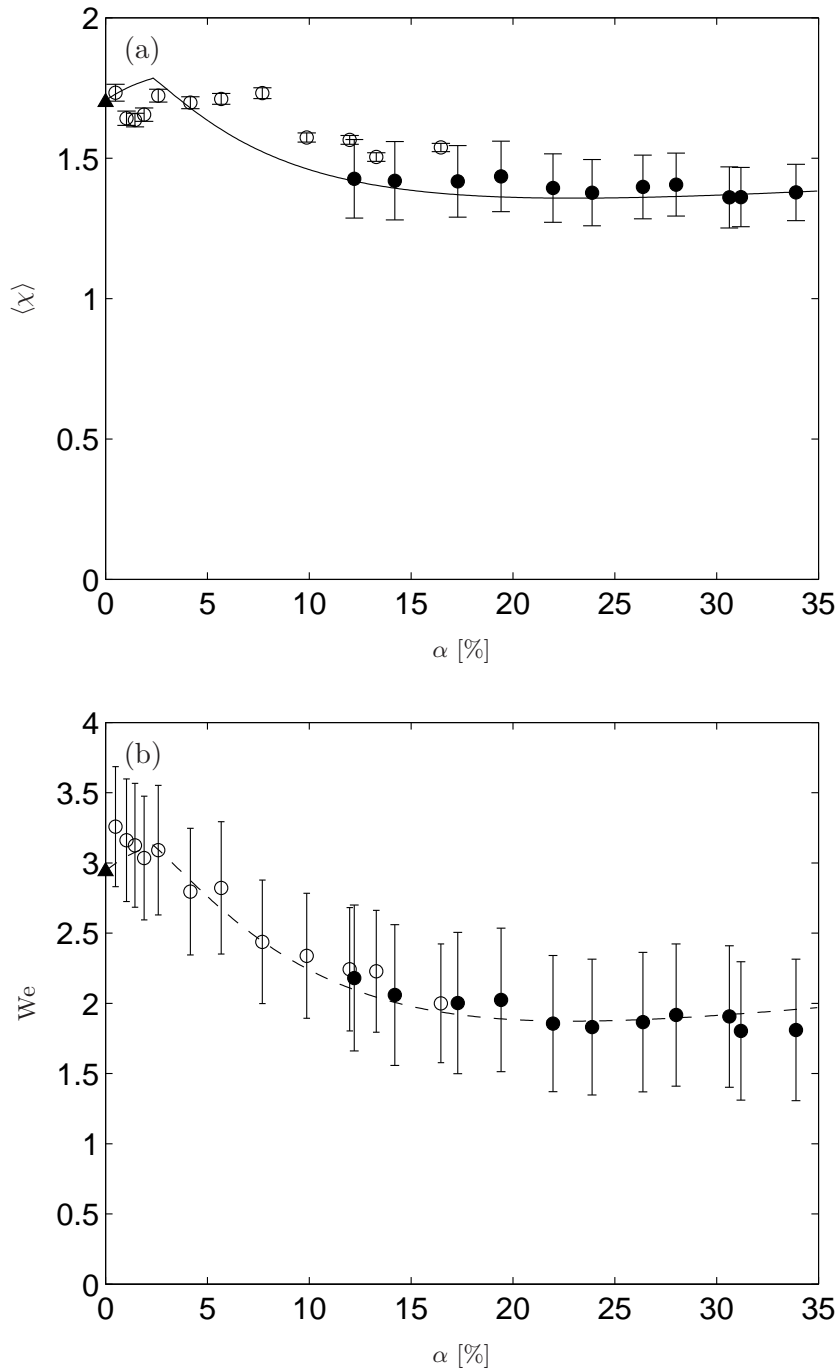


FIGURE 10. (a) Bubble average aspect ratio and (b) Weber number ($We = \rho_L \langle V_z \rangle^2 \langle d \rangle / \sigma$) versus gas volume fraction: \circ method using a fixed focal lens; \bullet method using a telecentric lens; \blacktriangle result for a single bubble from Riboux *et al.* (2010); — aspect ratio estimated from Eq. 3.6 (Legendre *et al.* 2012); -- Weber number determined from fitted data (eqs. 3.1, 3.2 and 3.5).

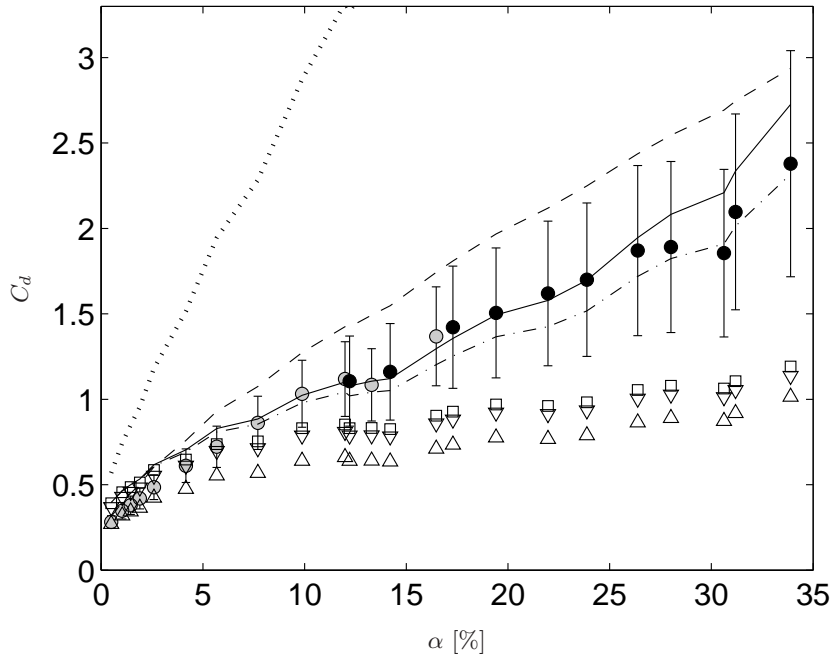


FIGURE 11. Experimental drag coefficient (Eq. 3.7) against gas volume fraction: \bullet method using a fixed focal lens; \bullet method using a telecentric lens. Drag coefficient for a single bubble of same equivalent diameter rising at its terminal velocity (Eq. 3.8): \square Mendelson (1967); ∇ Comolet (1979); \triangle Dijkhuizen *et al.* (2010). Drag coefficient accounting for the collective effect of the bubbles: $—$ Wallis (1961) (Eq. 3.9); $-.-$ Ishii & Chawla (1979) (Eq. 3.10); \dots Garnier *et al.* (2002) (Eq. 3.11); $---$ Roghair *et al.* (2011) (Eq. 3.12).

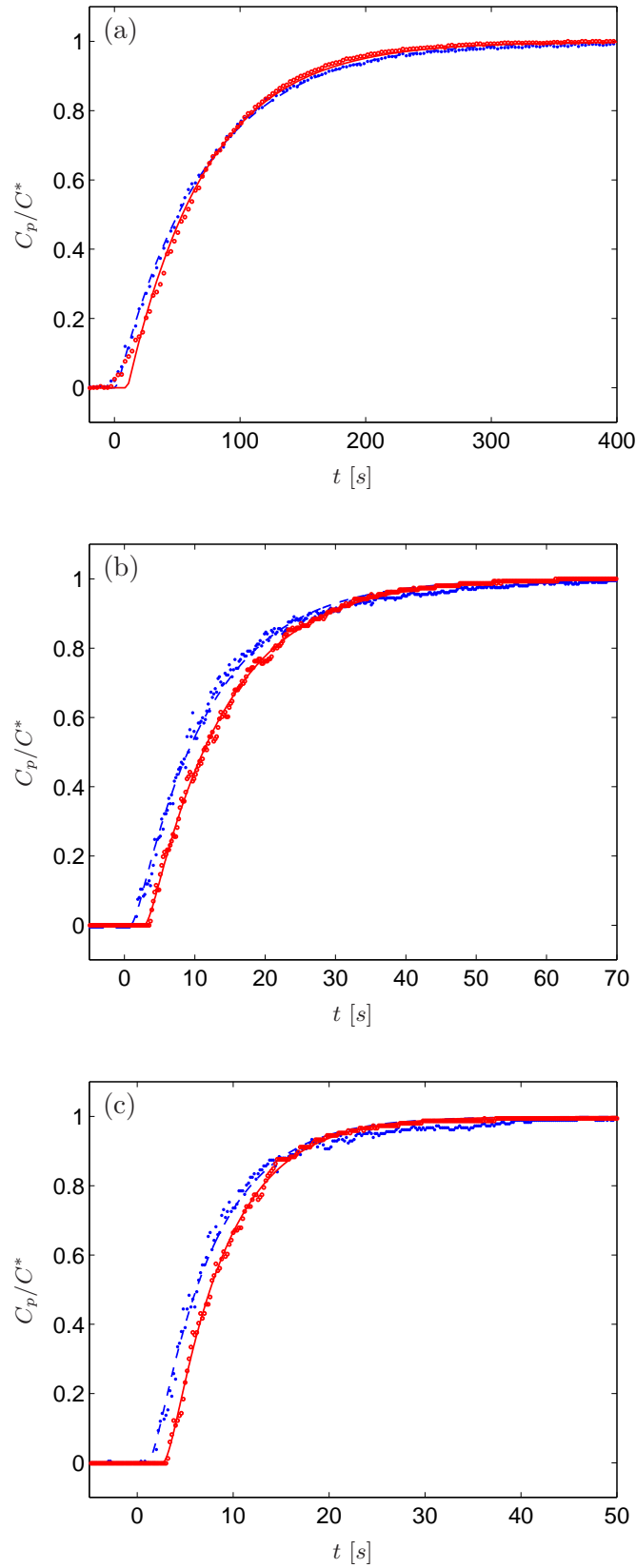


FIGURE 12. Typical measured time evolutions of the concentration of dissolved oxygen. (a) $\alpha = 1.46\%$, (b) $\alpha = 15.1\%$ and (c) $\alpha = 26.9\%$: \bullet lower probe and \circ upper probe. $-$ and $-$ equation (2.11) (Color online).

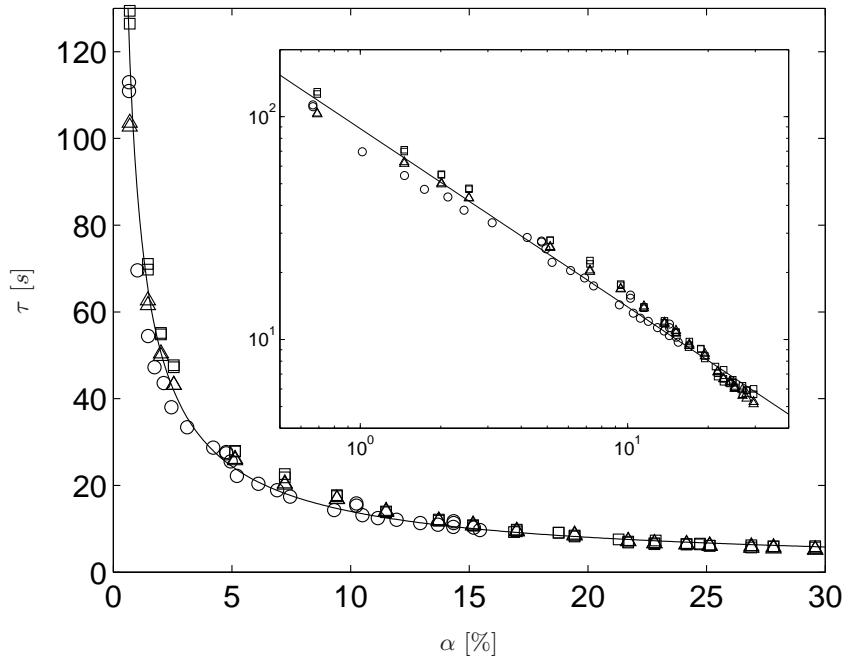


FIGURE 13. Time scale of the mass transfer versus the gas volume fraction: \square lower probe and \triangle upper probe; \circ Colombet *et al.* (2011) (using a single oxygen probe); — experimental fit (eq. 4.1). Insert: log-log representation.

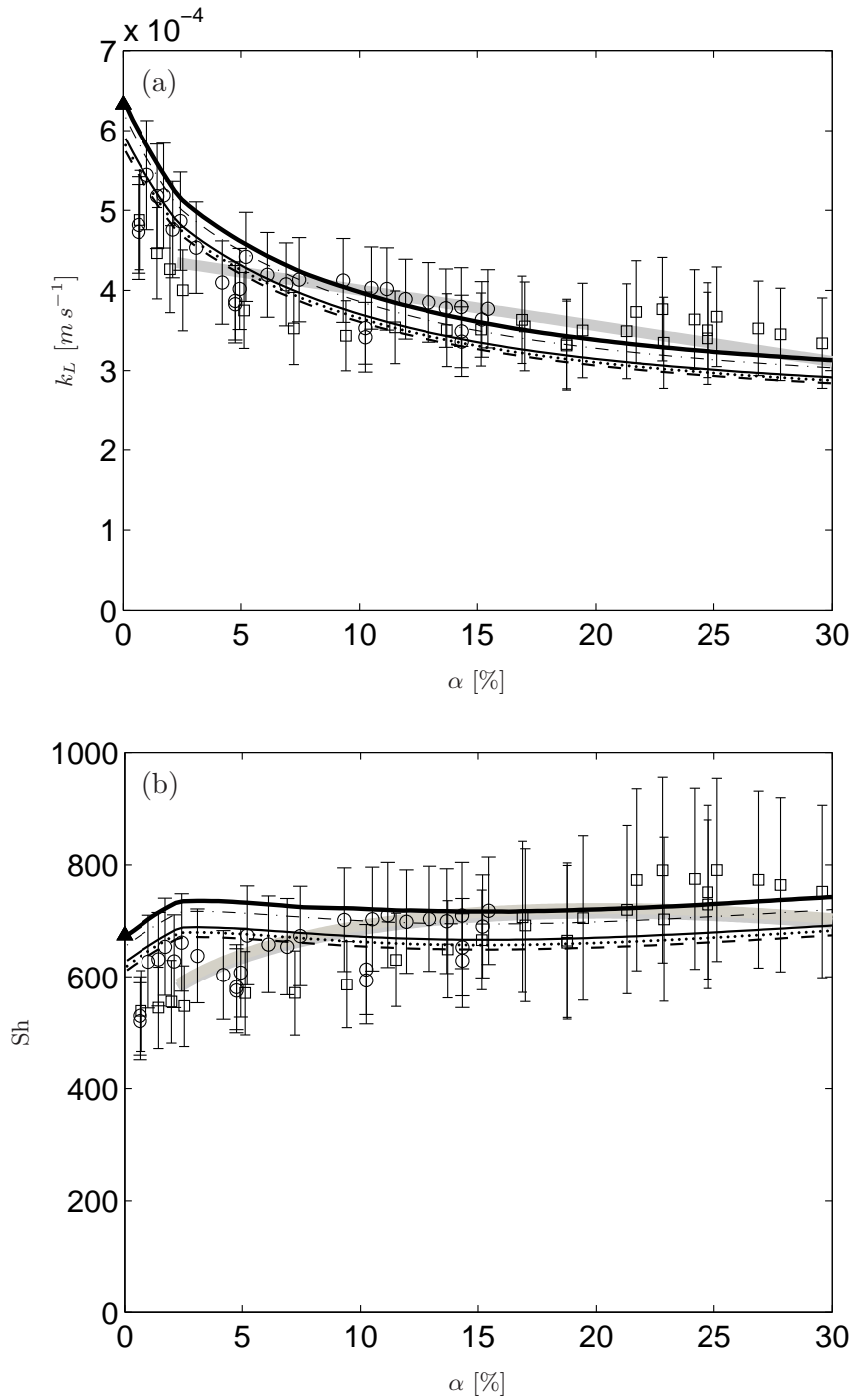


FIGURE 14. Mass transfer coefficient (a) and Sherwood number (b) versus gas volume fraction. Experiments: \square this work (average values) and \circ Colombet *et al.* (2011), --- empirical fits (eq. 4.3 and 4.5). Predictions for an isolated bubble: \blacktriangle single bubble (eqs. 4.12-4.13 with the parameters measured for an isolated bubble detached from a single capillary); -.- eq. (4.7) (Boussinesq 1905); \dots eq. (4.8) (Winnikow 1967); -- -- eq. (4.9) (Takemura & Yabe 1998); --- eq. (4.10) (Colombet *et al.* 2013); --- eqs. (4.12-4.13) (Figueroa & Legendre 2010).

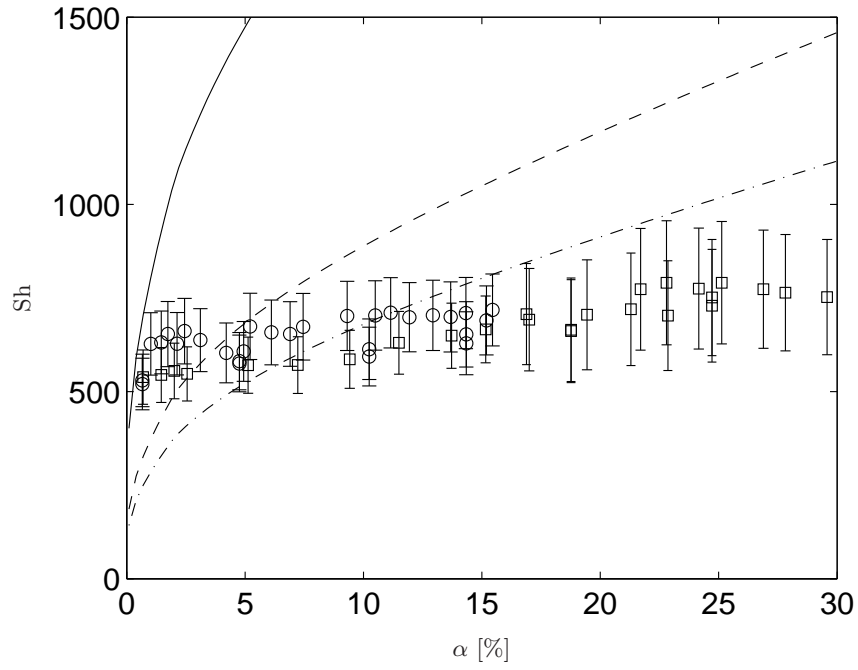


FIGURE 15. Comparison of the measured Sherwood number with mass transfer models for turbulent flows. Present experiments: same legend than in Fig. 14; Eqs. (4.14) and (4.15) with $- c_1 = 2/\sqrt{\pi}$ (Kawase *et al.* 1987), $-- c_1 = 0.523$ (Linek *et al.* 2004), $-. c_1 = 0.4$ (Lamont & Scott 1970).